molecular pharmaceutics

Article

pubs.acs.org/molecularpharmaceutics

Another Brick in the Wall. Validation of the σ_1 Receptor 3D Model by Computer-Assisted Design, Synthesis, and Activity of New σ_1 Ligands

Erik Laurini,[†] Domenico Marson,[†] Valentina Dal Col,[†] Maurizio Fermeglia,[†] Maria Grazia Mamolo,[‡] Daniele Zampieri,[‡] Luciano Vio,[‡] and Sabrina Pricl*[,†,§]

[†]Molecular Simulation Engineering (MOSE) Laboratory, Department of Industrial Engineering and Information Technology (DI3), University of Trieste, Via Valerio 10, 34127 Trieste, Italy

[§]INSTM Trieste Unit, University of Trieste, 34127 Trieste, Italy

[‡]Department of Chemical and Pharmaceutical Sciences, University of Trieste, Piazzale Europa 1, 34127 Trieste, Italy

Supporting Information

ABSTRACT: Originally considered an enigmatic polypeptide, the σ_1 receptor has recently been identified as a unique ligand-regulated protein. Many studies have shown the potential of σ_1 receptor ligands for the treatment of various diseases of the central nervous system (CNS); nevertheless, almost no information about the 3D structure of the receptor and/or the possible modes of interaction of the σ_1 protein with its ligands have been unveiled so far. With the present work we validated our σ_1 3D homology model and assessed its reliability as a platform for σ_1 ligand structure-based drug design. To this purpose, the 3D σ_1 model was exploited in the design of 33 new σ_1 ligands and in their ranking for receptor affinity by extensive molecular dynamics simulation-based free energy calculations. Also, the main interactions involved in receptor/ligand binding were analyzed by applying a per residue free energy deconvolution and *in silico* alanine scanning mutagenesis calculations. Subsequently, all compounds were synthesized in our laboratory and tested for σ_1 binding activity *in vitro*. The agreement between *in silico* and *in vitro* results confirms the reliability of the proposed σ_1 3D model in the *a priori* prediction of the affinity of new σ_1 ligands. Moreover, it also supports and corroborates the currently available biochemical data concerning the σ_1 protein residues considered essential for σ_1 ligand binding and activity.

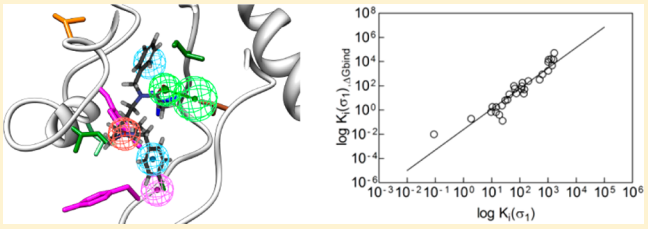

KEYWORDS: *σ_1 receptor, homology model, pharmacophore model, MM/PBSA, per-residue free energy decomposition, computational alanine scanning*

INTRODUCTION

Originally considered an enigmatic protein, the σ_1 receptor and its functions still remain quite elusive. Initially erroneously classified as opioid receptors,[1] two protein subtypes—namely, the σ_1 and σ_2 receptors—have been clearly identified so far,[2] but only the σ_1 receptor has been cloned.[3] σ receptors are widely distributed in the central nervous system (CNS) and the peripheral tissues.[4] The σ_1 protein shows a modulatory role on Ca^{2+} and K^+ channels and controls opioid analgesia and *N*-methyl-D-aspartate (NMDA), muscarinic, dopaminergic, and serotoninergic neurotransmission.[5] Moreover, σ_1 and, especially, σ_2 receptors were found overexpressed in several cancer cell lines,[6] a discovery that led to the development of σ receptor ligands as imaging tools and anticancer agents.[7,8]The endogenous ligand for σ receptors has not been unequivocally identified to date: some neurosteroids[9,10] (e.g., dehydroepiandrosterone sulfate and, particularly, progesterone) and *N*,*N*-dimethyltryptamine (DMT)[11] were suggested as putative endogenous ligands, but their affinities for σ receptors are too moderate for a definite identification. Also, the interaction of these receptors and the G-protein signaling pathway remains unclear. Until 2011, it was a common belief that there was no connection between σ receptors and G-protein; however, a recent work by Brimson[12] demonstrates that σ_1 receptor antagonists—but not agonists—show GTP- and suramin-sensitive high affinity binding, enlightening the association between G-proteins and the σ_1 receptor. Along with their diagnostic and curative role on tumors, σ ligands have been proposed as antiamnesics in memory and learning impairment, and as active agents for the prevention and treatment of neurodamage, schizophrenia, cocaine abuse, and other neurological disorders.[13] Furthermore, the σ_1 gene is known to be located on band p13 of the human chromosome 9, a region known to be related to many psychiatric disorders.[14]

In 1996, Kekuda and collaborators cloned the σ_1 receptor, a single polypeptide chain of 223 amino acids, for the first time.[15] Since then, no information was released about the three-

Received: April 26, 2012
Revised: September 25, 2012
Accepted: September 28, 2012
Published: September 28, 2012

dimensional (3D) structure of this receptor, this lack of evidence being mainly ascribable to the technical difficulty of obtaining a pure crystal from a membrane-bound protein. From the structural standpoint, the only information available mostly concerns the protein main structural motifs, which include an intracellular N-terminal end, two transmembrane spanning domains (residues 10−30 and 80−100) linked by an extracellular loop, and a partially arranged C-terminal end.[16] With the feeling that the 3D structure of the σ_1 protein is destined to remain experimentally unsolved, our group recently faced the problem of the σ_1 receptor structure from a molecular modeling perspective.[17] Thus, a σ_1 three-dimensional (3D) model was first generated and optimized by homology modeling techniques, and then refined exploiting data derived from 3D pharmacophore modeling, ligand docking, molecular dynamics-based affinity scoring, and mutagenesis experiments.[18−20] The reliability of the proposed σ_1 3D structure was preliminarily assessed by ranking a small series of bioactive σ_1 ligands for protein affinity using molecular dynamics (MD) simulations based on the MM/PBSA methodology.[21] The receptor/ligand binding constants determined *in silico* were found in agreement with the corresponding available experimental values. However, a thorough validation of the current 3D σ_1 homology model is undoubtedly required.

Thus, in this work we present an exhaustive validation of the predictive capability of our σ_1 3D model in computer-assisted drug design. Briefly, by exploiting a 3D pharmacophore model developed for σ_1 ligands[19] we designed 33 new σ_1 ligands endowed with affinity values for the receptor spanning 5 orders of magnitude. All these compounds were docked into the putative binding site of the σ_1 3D receptor model[17] using a pharmacophore-guided procedure and then ranked for affinity by MD-based free energy calculations. The binding modes of all compounds and the key receptor residues involved in each ligand binding were further assessed by applying a per residue deconvolution of the free energy of binding and *in silico* alanine scanning mutagenesis. Subsequently, all 33 compounds were synthesized in our laboratory and tested for σ_1 binding activity *in vitro*. Pleasingly, the *in silico*/*in vitro* results were found in agreement, ultimately confirming the reliability of the σ_1 3D model and its usefulness in computer-based design and development of new σ_1 ligands.

3D PHARMACOPHORE-BASED DESIGN OF NEW σ_1 LIGANDS

The initial step of the present work consisted of exploiting our 3D pharmacophore model (see Figure SI1 in the Supporting Information) for the *in silico* design of new σ_1 ligands.[19] Accordingly, starting from compounds **1e** and **2c**[17] (see Figure 1, top panels), we designed two new molecular series **1a−r** and **2a−l** (Figure 1, bottom panels) with a wide range of σ_1 receptor affinity values $K_i(\sigma_1)$, as shown in Table 1.

Quite interestingly, compounds belonging to series **1** are generally endowed with a lower affinity toward the σ_1 receptor than those of series **2**. This aspect can be explained by comparing, for instance, the mapping of two of the most active compounds of both series (i.e., **1f** $K_i(\sigma_1)_{3DPh}$ = 43.7 nM) and **2d** ($K_i(\sigma_1)_{3DPh}$ = 9.7 nM) on the corresponding 3D pharmacophore features, as shown in Figure 2.

The 3D pharmacophore model for σ_1 ligands shown in Figure 1 is characterized by five chemical features: one positive ionizable (PI) site, one hydrogen bond acceptor (HBA) group, two hydrophobic aromatic (HYAr) moieties, and one further

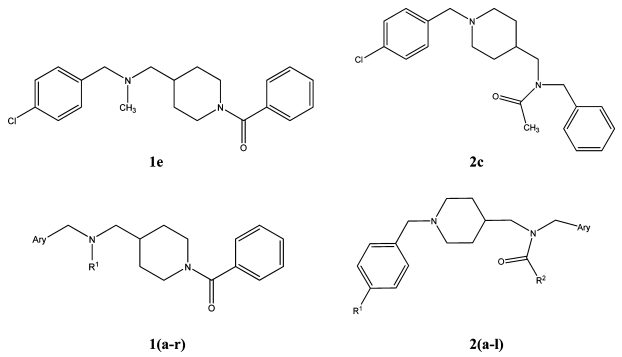

Figure 1. (Top) Chemical structure of compounds **1e** and **2c**. (Bottom) Molecular structures of compounds of series **1** and **2**.

hydrophobic (HY) site. Thus, when superposed on this pharmacophore model, compound **2d** maps all the chemical features with perfect overlap (Figure 2A): the phenyl ring matches the aromatic hydrophobic function, the chlorine atom fills the hydrophobic group of the model, and the basic nitrogen atom has the function of proton acceptor, while the carbonyl group matches the hydrogen bond feature. On the other hand, the chemical groups on compound **1f**, although suitable to fulfill all chemical requirements of the 3D pharmacophore, cannot be perfectly superposed to the corresponding pharmacophoric features due to a different molecular conformation and steric rigidity characterizing this molecule (Figure 2B).

ASSISTED-LIGAND DOCKING INTO THE σ_1 RECEPTOR 3D HOMOLOGY MODEL

The putative binding site and binding modes of all compounds **1a−r** and **2a−l** in the σ_1 receptor 3D homology model structure were retrieved taking advantage of (i) the currently available preliminary information on sequence-structure relationships and mutagenesis studies, (ii) the ligand-binding pharmacophore requirements, and (iii) the docking poses and receptor affinity ranking of compounds **1e** and **2c**.[17] To summarize briefly, a protein isoform missing residues 119−149 was found devoid of ligand binding capacity, and the conversion of residues Asp126 and Glu172 to glycine led to a severalfold reduction in ligand-binding function for the σ_1 receptor.[18] Moreover, our hydrophobicity analysis[17] identified, aside from the transmembrane (TM) domains, a third hydrophobic region matching the SBDLII (steroid binding domain-like II) region and centered on Asp188, a residue specifically photolabeled by [^{125}I]IACoc (3-iodo-4-azidococaine).[22] This protein region having been localized as a possible zone for ligand binding, a thorough search for a sequence satisfying the 3D pharmacophoric requirements[19] was performed and successfully retrieved. Thus, all compounds **1a−r** and **2a−l** were docked into the putative binding site of the σ_1 receptor 3D model. For each compound, in the corresponding set of docked ligand conformations a solution was found that best reproduced the key 3D pharmacophore requirements (see Figure 3). Each resulting receptor/ligand complex was then relaxed by energy minimization and MD simulations. Finally, the relevant values of the free energy of binding ΔG_{bind} between all compounds and the σ_1 receptor were evaluated by applying the well-known molecular mechanics/Poisson−Boltzmann surface area (MM/PBSA) computational ansatz,[21,23] as listed in Table 2.

Table 1. 3D Pharmacophore Predicted σ_1 Receptor Affinities $K_i(\sigma_1)_{3DPh}$ of compounds 1a−r and 2a−l

compd	Ary	R^1	$K_i(\sigma_1)_{3DPh}$ (nM)	compd	Ary	R^1	R^2	$K_i(\sigma_1)_{3DPh}$ (nM)
1a	phenyl	H	228	**1p**	pyridin-2-yl	Bz		810
1b	4-chlorophenyl	H	32.5	**1q**	pyridin-3-yl	Bz		1961
1c	4-methylphenyl	H	116	**1r**	pyridin-4-yl	Bz		785
1d	phenyl	CH_3	27.0	**2a**	phenyl	H	CH_3	24.1
1e	4-chlorophenyl	CH_3	66.7	**2b**	phenyl	H	phenyl	75.2
1f	4-methylphenyl	CH_3	43.7	**2c**	phenyl	Cl	CH_3	1.04
1g	phenyl	Bz	32	**2d**	phenyl	Cl	phenyl	9.7
1h	4-chlorophenyl	Bz	83	**2e**	4-chlorophenyl	H	CH_3	0.26
1i	4-methylphenyl	Bz	462	**2f**	4-chlorophenyl	H	phenyl	37.1
1j	pyridin-2-yl	H	520	**2g**	4-chlorophenyl	Cl	CH_3	20.4
1k	pyridin-3-yl	H	4433	**2h**	4-chlorophenyl	Cl	phenyl	25.7
1l	pyridin-4-yl	H	1148	**2i**	4-methylphenyl	H	CH_3	6.8
1m	pyridin-2-yl	CH_3	1186	**2j**	4-methylphenyl	H	phenyl	319
1n	pyridin-3-yl	CH_3	2683	**2k**	4-methylphenyl	Cl	CH_3	86.5
1o	pyridin-4-yl	CH_3	3731	**2l**	4-methylphenyl	Cl	phenyl	86.6

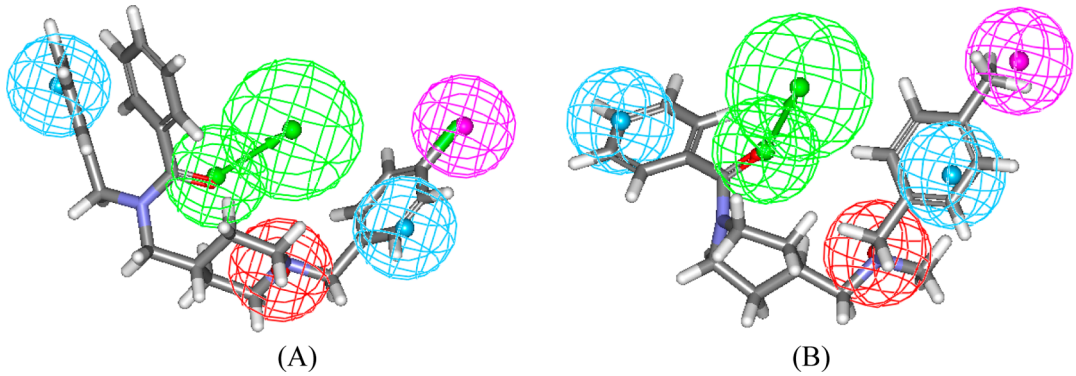

Figure 2. Pharmacophore mapping of **2d** (A) and **1f** (B). The 3D pharmacophore hypothesis features are portrayed as meshed spheres, color-coded as follows: red, positive ionizable (PI); light blue, hydrophobic aromatic (HYAr); pink, hydrophobic (HY); light green, hydrogen bond acceptor (HBA) (see text for more explanations).

Figure 3 shows three MD snapshots extracted from the corresponding equilibrated trajectories of **2e**, **1g**, and **1j** in complex with the σ_1 receptor, as an example. Among both series of compounds, **2e** is the molecule characterized by the highest MM/PBSA predicted affinity toward the σ_1 receptor, $K_i(\sigma_1)_{\Delta Gbind}$ = 0.01 nM (see Table 2), in agreement with the corresponding estimation from the 3D pharmacophore model ($K_i(\sigma_1)_{3DPh}$ = 0.26 nM, Table 1). From Figure 3A it is instructive to observe how, for **2e**, a hydrogen bond (HB) is established between the carbonyl oxygen of the ligand and the side-chain −OH group of Thr151 on the receptor. This HB, which persists throughout the entire MD simulation period, is characterized by an average dynamic length (ADL) of 1.82 ± 0.21 Å and yields a substantial contribution to binding (*vide infra* for a quantitative discussion of these data). A permanent salt bridge (SB, ADL = 3.81 ± 0.10 Å) is detected between the $-COO^-$ group of Asp126 on the receptor side and the piperidine $-NH^+$ moiety of **2e**. The 4-Cl-phenyl group of the compound is encased in a hydrophobic pocket, mainly lined by the side chains of Val171 and Ile128. An outer hydrophobic region accommodates the second phenyl ring of **2e**, with the contribution of residues Leu182, Ile178, and Tyr120. Also, this phenyl ring is further engaged in a parallel $\pi-\pi$ stacking interaction with Tyr120. The synergistic effect of all these stabilizing interactions is reflected in the highly negative (i.e., favorable) value of ΔG_{bind} between **2e** and the σ_1 protein (−15.12 kcal/mol, Table 2) and, hence, of the predicted subnanomolar value of the corresponding $K_i(\sigma_1)_{\Delta Gbind}$.

For compound **1g**, MM/PBSA calculations yield an intermediate affinity for the σ_1 receptor—$K_i(\sigma_1)_{\Delta Gbind}$ = 51.2 nM (see Table 2)—a value quite close to that predicted by the 3D pharmacophore model ($K_i(\sigma_1)_{3DPh}$ = 32 nM, Table 1). Figure 3B illustrates how the stable HB and the SB outlined for **2e** are still present, although the hydrogen donor on the receptor side in this case is the −NH group of the backbone peptide bond between Thr151 and Val152. Both these interactions, however, are somewhat weaker than for **2e**, as the corresponding ADL are 2.09 ± 0.12 Å (HB) and 4.53 ± 0.18 Å (SB), respectively. The hydrophobic pockets again enwrap two of the aromatic rings, residue Trp121 playing a role in determining a T-stacked $\pi-\pi$ interaction with one of the two aryl groups. However, the conformation of the molecule is such that the last phenyl ring is not mapped by any suitable pharmacophore feature of **1g**; correspondingly, this interaction is lost within the receptor binding site (Figure 3B). In line with this analysis, the presence of these less effective, albeit still favorable, interactions is reflected in the higher (less negative) value of the estimated free energy of binding (ΔG_{bind} = −9.95 kcal/mol, Table 2).

According to both 3D pharmacophore modeling and MM/PBSA simulations, compound **1j** is endowed with the lowest affinity toward the σ_1 receptor, with values of $K_i(\sigma_1)_{3DPh}$ = 520 nM and $K_i(\sigma_1)_{\Delta Gbind}$ = 52600 nM, respectively. In this case, the

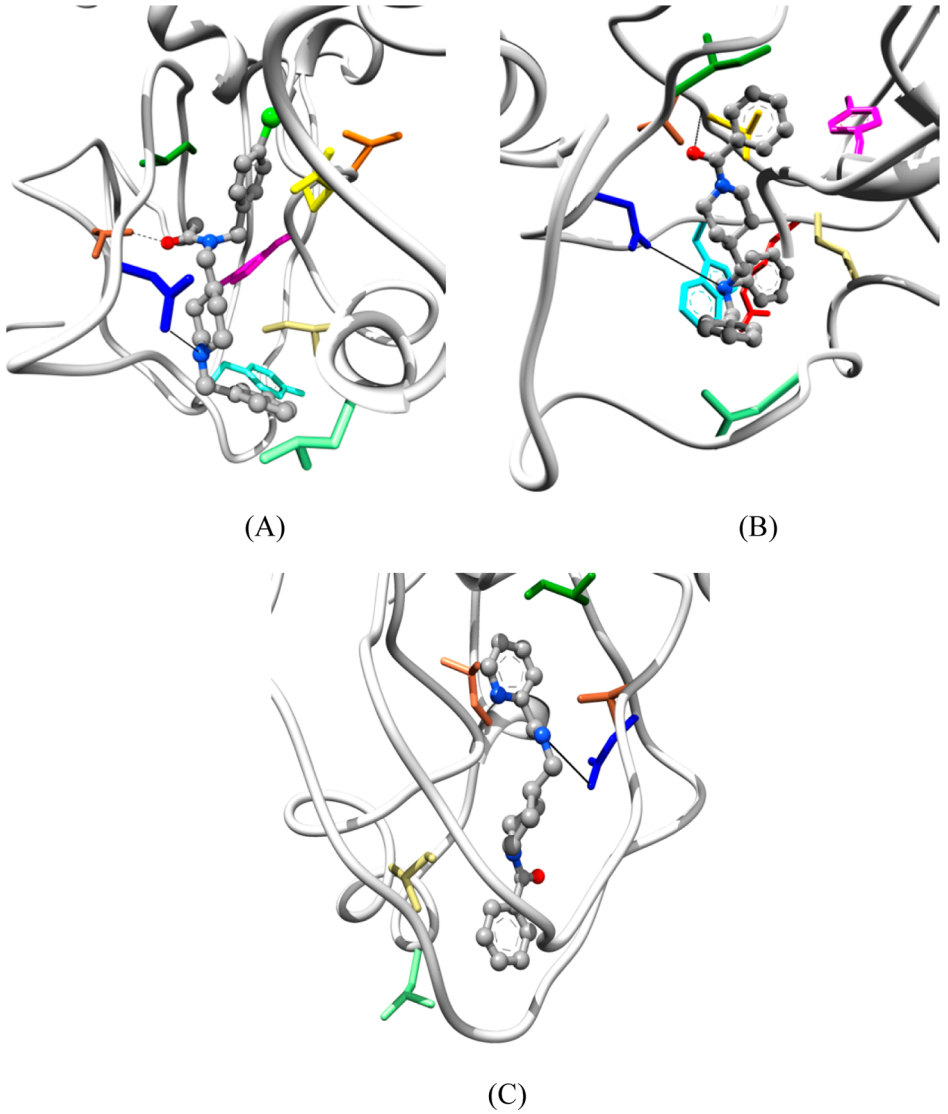

Figure 3. Details of the key interactions detected in the equilibrated MD snapshots of **2e** (A), **1g** (B), and **1j** (C) in complex with the σ_1 receptor 3D homology model. The main protein residues involved in ligand/receptor interactions are Arg119 (red), Tyr120 (aquamarine), Trp121 (cyan), Asp126 (blue), Ile128 (forest green), Thr151 (sienna), Val152 (gold), Val 171 (orange), Glu172 (yellow), Tyr173 (magenta), Ile178 (khaki), Leu182 (light green), and Leu186 (coral). Compounds **2e**, **1g**, and **1j** are shown in atom-colored sticks and balls: C, gray; O, red; N, blue; and Cl, green. H atoms are not shown, but H-bonds and salt bridges are indicated as black dotted and continuous lines, respectively. In all images, water molecules, ions, and counterions are not shown for clarity.

role exerted by Tyr120 and Thr151 in binding **1j** is negligible, while the two hydrophobic pockets described above are still able to accommodate the two aromatic moieties of this compound (Figure 3C). More importantly, the carbonyl group is positioned far too distant from any possible proton donor group on the receptor to set up any stabilizing HB bond. In agreement with these considerations, a very low activity is predicted for this compound, with a corresponding ΔG_{bind} value of −5.84 kcal/mol.

According to the present MM/PBSA analysis, the binding affinity of the two series of compounds **1** and **2** toward the σ_1 receptor is an enthalpy-driven process: indeed, panel A in Figure 4 shows that for both molecular sets the unfavorable entropic contribution $T\Delta S$ to ligand binding is overwhelmed by the favorable enthalpic component ΔH, resulting in an overall negative value of the free energy of binding ΔG_{bind}. It is also interesting to note that the higher MM/PBSA average σ_1 affinity value predicted for all compounds of series **2** originates solely from the difference in the enthalpic contributions between the two molecular sets ($\Delta\Delta H = \Delta H(\mathbf{2}) - \Delta H(\mathbf{1}) = -4.91$ kcal/mol), as the corresponding difference in the entropic terms is significantly smaller ($\Delta T\Delta S = T\Delta S(\mathbf{2}) - T\Delta S(\mathbf{1}) = 1.56$ kcal/(mol K)).

The calculated ΔG_{bind} values are encouraging also in the light of the balance among the energy terms contributing to them. As observed in many other drug/receptor complex simulations including our own studies,[24] the favorable contribution of the electrostatic interactions between the σ_1 protein and compounds **1a**−**r** and **2a**−**l** (ΔE_{ele}) is more than compensated by the electrostatic desolvation free energy upon complexation (ΔG_{PB}), so that the total electrostatic term ($\Delta E_{ele} + \Delta G_{PB}$) contributes unfavorably to the binding (see Figure 4B). Interestingly, several recent papers have demonstrated that (natural) receptor−ligand pairs often show suboptimal electrostatic interactions that may be optimized, leading to increased affinity.[25−29] On the contrary, van der Waals interactions

Table 2. Enthalpy (ΔH), Entropy ($-T\Delta S$), Free Energy of Binding (ΔG_{bind}), and Corresponding $K_i(\sigma_1)_{\Delta Gbind}$ Values[a] for Compounds 1a−r and 2a−l and the σ_1 Receptor Homology Model,[22] as Estimated Using the MM/PBSA Approach[b]

compd	ΔH (kcal/mol)	$-T\Delta S$ (kcal/(mol K))	ΔG_{bind} (kcal/mol)	$K_i(\sigma_1)_{\Delta Gbind}$ (nM)	compd	ΔH (kcal/mol)	$-T\Delta S$ (kcal/(mol K))	ΔG_{bind} (kcal/mol)	$K_i(\sigma_1)_{\Delta Gbind}$ (nM)
1a	−36.29 (0.19)	−26.36 (0.34)	−9.93 (0.39)	53.0	**1p**	−31.89 (0.16)	−23.03 (0.37)	−8.86 (0.40)	322
1b	−34.39 (0.21)	−23.87 (0.32)	−10.52 (0.38)	19.6	**1q**	−30.92 (0.18)	−23.67 (0.34)	−7.25 (0.38)	4870
1c	−36.18 (0.17)	−25.75 (0.31)	−10.43 (0.35)	22.8	**1r**	−29.97 (0.20)	−22.11 (0.33)	−7.86 (0.39)	1740
1d	−35.02 (0.18)	−24.62 (0.35)	−10.40 (0.39)	24.0	**2a**	−38.31 (0.20)	−25.81 (0.35)	−12.50 (0.40)	0.69
1e	−37.90 (0.18)	−26.71 (0.30)	−10.02 (0.35)	6.32	**2b**	−39.01 (0.15)	−26.19 (0.36)	−12.82 (0.39)	0.40
1f	−36.21 (0.20)	−25.09 (0.31)	−11.12 (0.37)	7.12	**2c**	−38.81 (0.19)	−25.54 (0.33)	−11.31 (0.38)	0.19
1g	−33.19 (0.16)	−23.24 (0.35)	−9.95 (0.38)	51.2	**2d**	−38.39 (0.19)	−24.91 (0.33)	−13.48 (0.38)	0.13
1h	−32.60 (0.20)	−23.39 (0.36)	−9.21 (0.41)	178	**2e**	−40.83 (0.21)	−25.71 (0.30)	−15.12 (0.37)	0.01
1i	−33.38 (0.19)	−24.37 (0.33)	−9.01 (0.38)	250	**2f**	−37.76 (0.17)	−25.97 (0.35)	−11.79 (0.39)	2.30
1j	−30.33 (0.18)	−24.49 (0.35)	−5.84 (0.39)	52600	**2g**	−38.33 (0.19)	−26.38 (0.34)	−11.95 (0.39)	1.75
1k	−29.89 (0.21)	−23.02 (0.31)	−6.87 (0.37)	9250	**2h**	−37.04 (0.18)	−25.11 (0.36)	−11.93 (0.40)	1.81
1l	−30.69 (0.17)	−22.43 (0.36)	−8.26 (0.40)	880	**2i**	−38.61 (0.19)	−26.09 (0.35)	−12.52 (0.40)	0.67
1m	−29.88 (0.21)	−23.35 (0.31)	−6.53 (0.37)	16400	**2j**	−33.95 (0.18)	−24.35 (0.32)	−9.60 (0.37)	92.5
1n	−29.24 (0.18)	−22.65 (0.32)	−7.75 (0.37)	14800	**2k**	−34.61 (0.19)	−25.03 (0.31)	−9.58 (0.36)	95.6
1o	−28.87 (0.22)	−22.27 (0.32)	−6.60 (0.39)	14600	**2l**	−34.49 (0.21)	−24.62 (0.35)	−9.87 (0.41)	58.6
PTZ	−27.56 (0.22)	−17.54 (0.39)	−10.02 (0.45)	45.5	**HAL**	−35.17 (0.19)	−24.56 (0.38)	−10.61 (0.42)	16.8

[a]The $K_i(\sigma_1)$ values were obtained from the corresponding ΔG_{bind} values using the relationship $\Delta G_{bind} = -RT \ln(1/K_i)$. [b]The values of two σ_1 ligand reference compounds, (+)-pentazocine (PTZ) and haloperidol (HAL), are also reported for comparison. Errors are given in parentheses as standard errors of the mean (SEM).

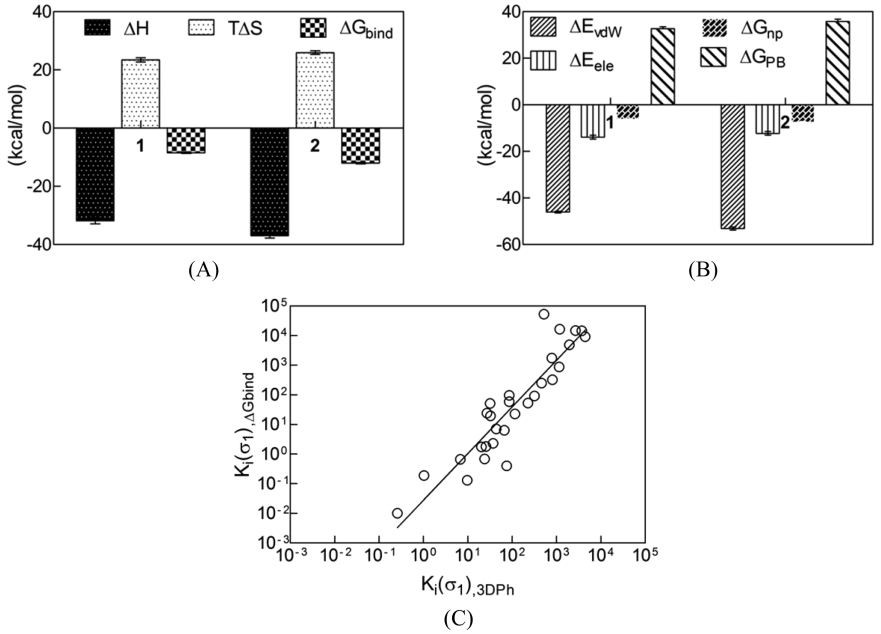

Figure 4. (A) Average MM/PBSA values of the enthalpy (ΔH), entropy ($T\Delta S$), and free energy of binding (ΔG_{bind}) for compound series **1** and **2** in complex with the σ_1 receptor. (B) Average values of the enthalpic components of ΔG_{bind} (van der Waals term ΔE_{vdW}, electrostatic term ΔE_{ele}, polar solvation term ΔG_{PB}, and nonpolar solvation term ΔG_{np}) for compound series **1** and **2** in complex with the σ_1 receptor (see Experimental Section for explanations). (C) Correlation between the σ_1 affinity constant K_i values for compounds **1a−r** and **2a−l** estimated using the 3D pharmacophore model ($K_i(\sigma_1)_{3DPh}$) and the MM/PBSA methodology ($K_i(\sigma_1)_{\Delta Gbind}$).

(ΔE_{vdW}) contribute favorably to the binding affinity of **1a−r** and **2a−l** toward the receptor, as does the nonpolar part of the solvation free energy (ΔG_{np}), again in agreement with other studies mentioned above[23−29] (Figure 4B). Therefore, for both **1** and **2** molecular series, the favorable binding free energy for receptor/ligand complex formation stems predominantly from the nonpolar terms (ΔE_{vdW} + ΔG_{np}), while the polar interactions provide most of all the directional constraint for the complexation, that is, the relative positions of the molecules.

The analysis of the entire MD simulation trajectories for all 33 compounds in complex with the σ_1 receptor 3D model further reveals that the overall conformation of the protein backbone undergoes only minimal global conformational changes upon complex formation with the different compounds, while a rearrangement of the side chains of several residues lining the receptor binding site is required for ligand binding. In its uncomplexed form, the σ_1 model structure remained stable for the entire 10 ns MD trajectory, as testified by the small root-mean-square deviation (RMSD) values of the backbone atom positions with respect to those of the initial

structure. The same parameter showed very low fluctuations during both MD equilibration and data harvesting steps also for all receptor/ligand complexes (see Figure SI3 in the Supporting Information), indicating that the presence of a bound ligand does not result in large protein structural deviations. The first part of Table 3 reports the average RMSDs of the binding site region of the σ_1 receptor (i.e., from residue 100 to residue 200) determined between average structures of the proteins in the unbound and bound states for **2e**, **1g**, and **1j** as an example: this region deviates by very small amounts, confirming that the σ_1 binding pocket does not experience a significantly larger-than-average conformational change upon complex formations with ligands **1** and **2**.

Table 3. Average Root-Mean-Square Deviations (RMSDs) of the Binding Site of the σ_1 Protein in Complex with 2e, 1g, and 1j with Respect to the Unbound Protein and to Each Alternative Complex[a]

2e	1g	1j	2e/1g	2e/1j	1g/1j
0.9	1.6	2.1	2.5	4.2	3.5

[a]All values are reported in Å.

These aspects can be further inspected and quantified considering the superposition of equilibrated snapshots extracted from the MD trajectory of the receptor in complex with compounds **2e**, **1g**, and **1j** reported in Figure 5 and the relevant RMSD values listed in the rightmost three columns of Table 3. This evidence confirms that the putative binding site of the σ_1 receptor is able to accommodate all ligands of series **1** and **2** with no major conformational readjustments, the difference in affinity toward the different compounds being ascribable to a better/worse rearrangement of the binding pocket residue side chains.

In concluding this section it is interesting to note that the affinity values of all 33 compounds toward the σ_1 receptor predicted by the 3D pharmacophore model are in good agreement with the corresponding values obtained from the MM/PBSA scoring, with a correlation coefficient of $R^2 = 0.84$, as shown in Figure 4C. The quality of the overall linear correlation between these two $K_i(\sigma_1)$ data sets constitutes a first step toward the validation of the σ_1 3D homology model and the location of its putative binding site.

RESIDUE-BASED DESCRIPTION OF LIGAND BINDING TO σ_1: PER RESIDUE BINDING FREE ENERGY DECOMPOSITION AND COMPUTATIONAL ALANINE SCANNING

Per Residue Binding Free Energy Decomposition. Insight into the origin of binding of σ_1 to compounds **1** and **2** at an atomistic level may be obtained by decomposing the total free energy of binding ΔG_{bind} in terms of contributions from structural subunits of both binding partners. The molecular mechanics/generalized Born surface area (MM/GBSA),[29] an attractive variant to MM/PBSA in which the electrostatic contribution to the solvation free energy is determined using a generalized Born (GB) model, allows the decomposition of the electrostatic solvation free energy into atomic contributions in a straightforward manner. This, in turn, permits an easy and rapid per residue binding free energy decomposition (PRBFED), yielding the residue-based ΔH_{GB} values required for the detailed study of the ligand/protein interactions at each single amino acid level, including the backbone atoms. Therefore, we proceeded in our study of the binding modes of compounds **1a**−**r** and **2a**−**l** to the σ_1 receptor by applying PRBFED to the analysis of those residues that, as qualitatively discussed above (Figure 3), are predicted to be important for ligand binding to the protein.

Figure 6 illustrates the results of the PRBFED analysis obtained for compounds **2e**, **1g**, and **1j**, again taken as a proof of concept as they constitute examples of σ_1 high affinity (**2e**), intermediate affinity (**1g**), and very low affinity (**1j**) ligands, respectively. As can be seen from Figure 6, in all cases three clusters of residues (I, II, and III) are identified, centered around Glu123, Thr151, and Val177, respectively. In the case of **2e** (Figure 6A), according to analysis of the corresponding MD trajectory (Figure 3A,B) the side chain of Asp126 is engaged in a fundamental salt bridge with the piperidine $-NH^+$ moiety of the compound; indeed, this residue is responsible for the −2.54 kcal/mol favorable contribution to binding, mostly provided by

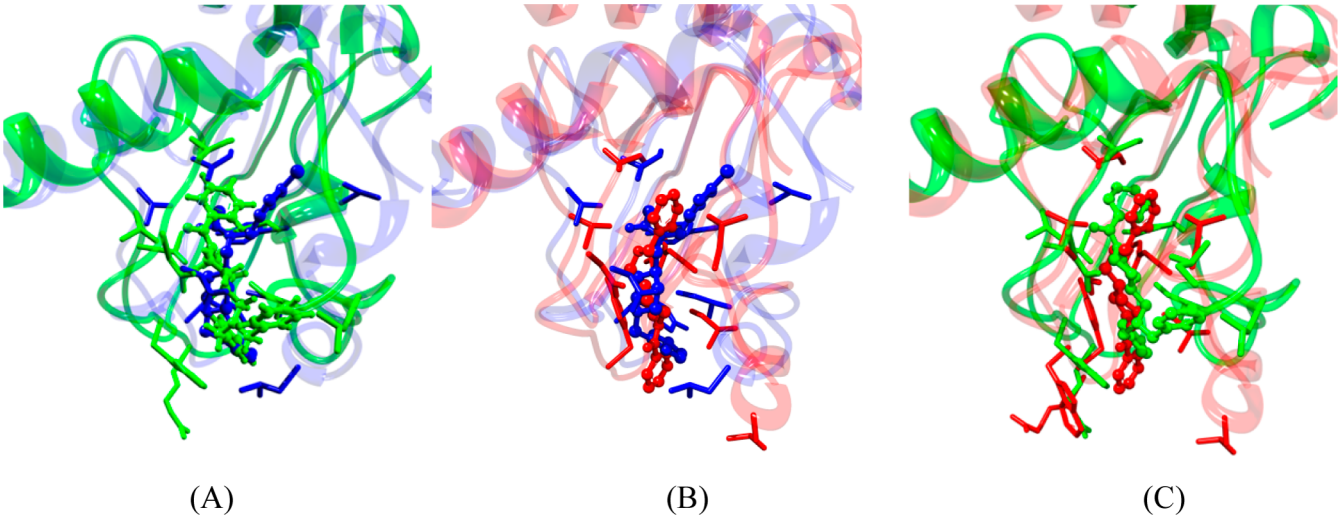

Figure 5. Superposition of equilibrated MD snapshots of the σ_1 receptor in complex with (A) **2e** (blue) and **1g** (green), (B) **2e** (blue) and **1j** (red), and (C) **1g** (green) and **1j** (red). The images are zoomed views of the receptor binding site. The ligands are portrayed in sticks and balls colored according to the protein in the corresponding complex. Water, ions, and counterions are not shown for clarity.

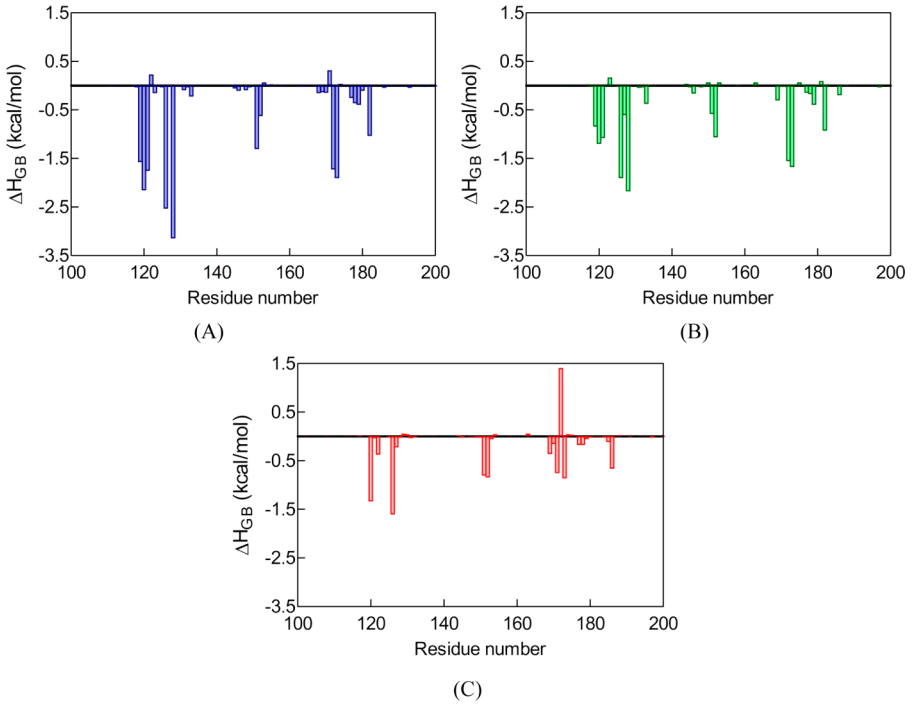

Figure 6. Per residue binding free energy decomposition for σ_1 receptor in complex with **2e** (A), **1g** (B), and **1j** (C). Only σ_1 amino acids from position 100 to 200 are shown, as for all the remaining protein residues the contribution to ligand binding is irrelevant.

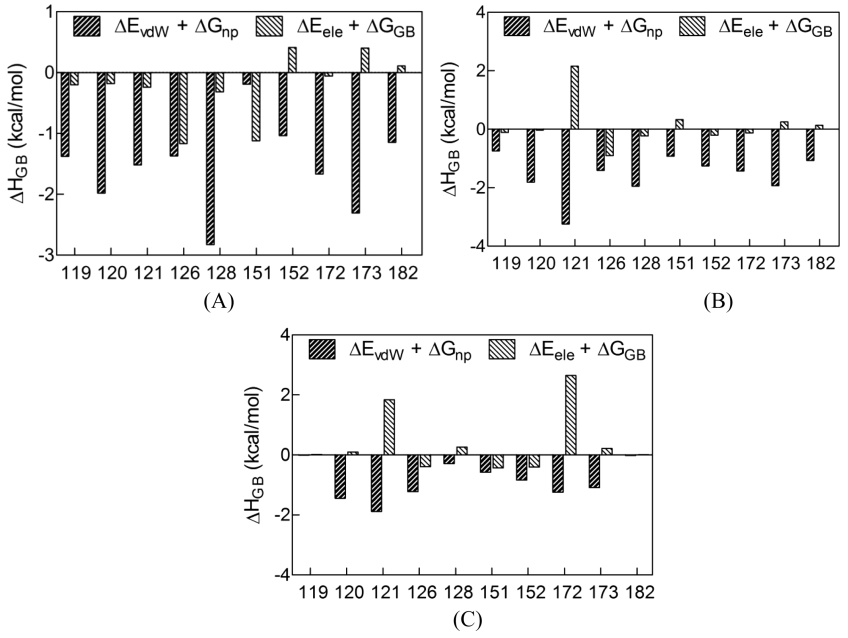

Figure 7. Decomposition of ΔH_{GB} on a per residue basis into contribution of the nonpolar ($\Delta E_{vdW} + \Delta G_{np}$) and polar ($\Delta E_{ele} + \Delta G_{np}$) terms for residues of the σ_1 receptor in complex with **2e** (A), **1g** (B), and **1j** (C). Only those residues for which $|\Delta H_{GB}| \geq 1$ kcal/mol are shown in the respective panels.

stabilizing electrostatic interactions. The stable hydrogen bond detected between the −CO group of **2e** and the side chain −OH group of Thr151 is responsible for the favorable −1.31 kcal/mol contribution provided by the electrostatic interactions. The PRBFED approach then confirms that residues belonging to the two major clusters yield the required van der Waals and hydrophobic interactions to favorably encase the aromatic portions of the ligand: e.g., Arg119 (−1.58 kcal/mol), Tyr120 (−2.16 kcal/mol), Trp121 (−1.76 kcal/mol), and Ile128 (−3.15 kcal/mol) of cluster I, and Glu172 (−1.73 kcal/mol), Tyr 173 (−1.91 kcal/mol), and Leu182 (−1.04 kcal/mol) of cluster II, respectively.

Panel B in Figure 6 illustrates the PRBFED results for compound **1g**. The presence of weaker (i.e., longer) SB and HB interactions detected along the **1g**/σ_1 MD trajectory (Figure 3C,D) is confirmed by the lower ΔH_{GB} values of the residues involved: −1.91 kcal/mol (SB) for Asp126 and −1.07 kcal/mol (HB) for Val152, respectively. The minor entity of the

dx.doi.org/10.1021/mp300233y | *Mol. Pharmaceutics* 2012, 9, 3107−3126

contributions to binding from residues belonging to clusters I and II (120−128 and 171−182) supports the evidence that part of the hydrophobic and van der Waals interactions are lost in this ligand/protein complex. Of note, the proposed T-stacked $\pi-\pi$ interaction of Trp121 with one of the two aryl groups of **1g** is captured by the PRBFED analysis, according to which the contribution afforded by this residue to binding is equal to −1.08 kcal/mol.

In our predictions, compound **1j** is the ligand characterized by the lowest affinity for the σ_1 receptor within both molecular series **1** and **2**. The PRBFED results shown in panel C of Figure 6 justify these calculations. While the presence of a salt bridge between the $-NH^+$ moiety of **1j** and the $-COO^-$ of Asp126 is preserved, providing a favorable contribution to binding of −1.61 kcal/mol, the absence of any H-bond between the −CO group of **1j** and any possible acceptor group on the receptor is responsible for the small contributions to binding from residues of cluster II (e.g., Thr151, −0.81 kcal/mol). Some residues of clusters I and II are still able to provide some favorable contribution to complex formation, although the reorientation of Glu172 side chain upon binding **1j** is in part responsible for the +1.41 kcal/mol unfavorable dispersion/electrostatic contribution to the binding made by this amino acid.

To gain additional insights into the different contributions to the binding free energy change, the per residue ΔH_{GB} values can be further decomposed into the nonpolar terms (i.e., the van der Waals energy ΔE_{vdW} and the nonpolar term of the solvation free energy ΔG_{np}) and the sum of the Coulombic interaction and the polar solvation free energy ($\Delta E_{ele} + \Delta G_{GB}$). Figure 7 depicts the ΔH_{GB} decomposition for the **2e**/, **1g**/, and **1j**/σ_1 complexes discussed above. The sum of electrostatic interactions in the gas phase and the change of the polar part of the solvation free energy is shown instead of the separate contributions, since, in most cases, the numbers are strongly anticorrelated.

Qualitatively, major differences are obvious among residues located in the binding site in the case of high, intermediate, and low affinity ligands, respectively. For compound **2e** ($K_i(\sigma_1)_{\Delta G bind}$ = 0.01 nM), stabilizing van der Waals and nonpolar interactions, reinforced by favorable overall electrostatic/desolvation terms, prevail for almost all residues lining the σ_1 binding pocket (Figure 7A). Interestingly, the overall stabilization of the salt bridge of **2e** with Asp126 (ΔG_{GB} = −2.54 kcal/mol, see PRBFED analysis) is almost equivalently contributed by the dispersive ($\Delta E_{vdW} + \Delta G_{np}$ = −1.37 kcal/mol) and electrostatic ($\Delta E_{ele} + \Delta G_{GB}$ = −1.17 kcal/mol) components, while the pharmacophoric H-bond involving the side chain of Thr151 (ΔG_{GB} = −1.31 kcal/mol) mainly gains from a favorable electrostatic interaction ($\Delta E_{ele} + \Delta G_{GB}$ = −1.12 kcal/mol while $\Delta E_{vdW} + \Delta G_{np}$ = −0.19 kcal/mol). Figure 7A also confirms the dominant role played by the hydrophobic (i.e., overall nonpolar) interactions in binding of **2e** to σ_1, well exemplified by the values of $\Delta E_{vdW} + \Delta G_{np}$ for residues Arg119 (−1.38 kcal/mol, ΔH_{GB} = −1.58 kcal/mol), Tyr120 (−1.98 kcal/mol, ΔH_{GB} = −2.16 kcal/mol), Trp121 (−1.52 kcal/mol, ΔH_{GB} = −1.76 kcal/mol), Ile128 (−2.83 kcal/mol, ΔH_{GB} = −3.15 kcal/mol), Glu172 (−1.67 kcal/mol, ΔH_{GB} = −1.73 kcal/mol), Tyr 173 (−2.31 kcal/mol, ΔH_{GB} = −1.91 kcal/mol), and Leu182 (−1.15 kcal/mol, ΔH_{GB} = −1.04 kcal/mol).

In the case of compound **1g** ($K_i(\sigma_1)_{\Delta G bind}$ = 51.2 nM), the dispersive forces benefit by a lower synergistic interaction with the polar terms of ΔH_{GB} with respect to the case of **2e** (Figure 7B). Notably, while the salt bridge between **1g** and Asp126, although decreased in strength (ΔH_{GB} = −1.91 kcal/mol), shows a relative contribution from the different ΔH_{GB} components which parallels that discussed for **2e** (i.e., $\Delta E_{vdW} + \Delta G_{np}$ amounts to approximately 74% of the total ΔH_{GB}), the other, distinctive pharmacophoric element (i.e., H-bond with Val152) not only is weaker but features contributions from the two main ΔH_{GB} components in a reverse trend with respect to **2e** ($\Delta E_{vdW} + \Delta G_{np}$ = −1.26 kcal/mol and $\Delta E_{ele} + \Delta G_{GB}$ = −0.20 kcal/mol, respectively). Of importance is the quantification of the $\pi-\pi$ stacking interaction between one aromatic moiety of **1g** and the side chain of Trp121 (ΔH_{GB} = −1.08 kcal/mol), for which the dispersive and the electrostatic terms show strong contributions of opposite sign ($\Delta E_{vdW} + \Delta G_{np}$ = −3.24 kcal/mol and $\Delta E_{ele} + \Delta G_{GB}$ = +2.16 kcal/mol, respectively).

Lastly, for compound **1j** ($K_i(\sigma_1)_{\Delta G bind}$ = 52600 nM) both the number of useful contacts with the amino acids belonging to the putative σ_1 binding site and also the overall intensity of the interactions between these residues and the ligand are highly diminished with respect to those characterizing compounds **2e** and **1g** discussed above. Also, at some specific positions already identified during PRFEBD analysis (e.g., Trp121 and Glu172), a gain in favorable van der Waals interactions and the nonpolar part of solvation free energy is overcompensated by unfavorable contributions from the $\Delta E_{ele} + \Delta G_{GB}$ components of ΔH_{GB}.

Computational Alanine Scanning Mutagenesis. The MD simulations performed in the MM/PBSA framework of theory can be further employed to perform the so-called computational alanine scanning (CAS) mutagenesis,[30,31] in which the absolute binding free energy is calculated for the wild type protein, as well as for several mutants in which one residue has been replaced by an alanine. Aside from yielding information complementary to that obtained from a PRBFED analysis, the difference in the binding free energy of the wild type and of the mutants estimated by CAS may be directly compared with the results of an experimental alanine scanning (ASM) mutagenesis. Undoubtedly, in the CAS approach it is questionable whether simply modifying a given side chain to alanine in the corresponding MD simulation trajectory of the wild type system can lead to a good representation of the conformational space of the mutant, since no eventual conformation induced by the mutation is investigated. However, it is also questionable how the binding free energy contribution of a given side chain in the wild type complexation may be always representative of the change in the binding free energy upon mutation, since the conformational modifications induced by the mutations are not included in the model either and since, for instance, the modification of the solvation free energy of close side chains upon mutation is not directly evaluated. Also, contrarily to the total free energy, the free energy components are not state functions, and the values of these contributions are thus dependent on the decomposition scheme adopted. Obviously, both CAS and the PRBFED methods cannot be expected to provide results exactly comparable to experimental values obtained from an experimental ASM; nonetheless, the application of both methodologies can give a good, preliminary indication of which protein residues play a key role in ligand binding, ultimately enabling the biochemist to avoid trial-and-error tests and perform targeted ASM experiments with the obvious advantages of cost and time saving.

Table 4. Computational Alanine Scanning (CAS) Mutagenesis Results for the σ_1 Receptor in Complex with Ligands 2e, 1g, and 1j[a]

		$\Delta\Delta G_{bind} = \Delta G_{bind,wt} - \Delta G_{bind,mut}$						
compd	$\Delta G_{bind,wt}$	D126A	I128A	T151A	V152A	E172A	Y173A	L182A
2e	−15.12 (0.37)	−3.69 (0.42)	−2.27 (0.43)	−0.67 (0.38)	−0.56 (0.40)	−2.04 (0.37)	−1.79 (0.38)	−1.11 (0.37)
1g	−9.95 (0.38)	−3.25 (0.39)	−1.35 (0.40)	−0.71 (0.39)	−0.45 (0.39)	−1.19 (0.40)	−2.03 (0.41)	−0.79 (0.43)
1j	−5.84 (0.39)	−2.82 (0.43)	−0.12 (0.42)	−0.57 (0.38)	−0.39 (0.43)	−0.21 (0.39)	−1.27 (0.38)	0.02 (0.44)

[a]All values are in kcal/mol. Errors are given in parentheses as standard errors of the mean (SEM).

Scheme 1

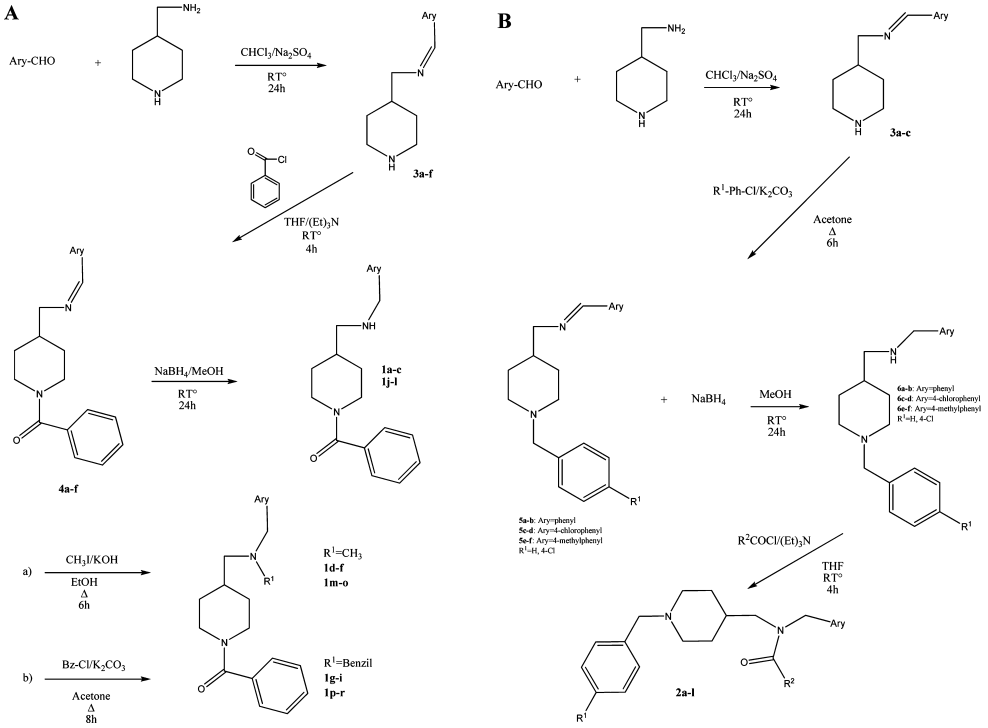

The CAS was applied to all compounds **1a−r** and **2a−l**; for the sake of brevity and in keeping with the previous discussion, Table 4 gives the results of the CAS for compounds **2e**, **1g**, and **1j** only. Note that, according to the definition adopted in this work (see also Experimental Section for more explanations), a negative value of $\Delta\Delta G_{bind}$ corresponds to a residue for which the wild type (wt) side chain is more favorable to the binding than an alanine side chain. From the values listed in Table 4, the pivotal role exerted by Asp126 in ligand binding is clearly attested by the highly unfavorable free energy of binding of the Ala126 σ_1 mutant with respect to the wt protein. Also, Tyr173 is confirmed to play a substantial role in the complex stabilization for each compound. Interestingly, residues Ile128 and Leu182 afford a significant contribution to the stabilization of the protein/ligand complex for those ligands with high or intermediate affinity (**2e** and **1g**) but seem to be less critical for compounds endowed by a poor affinity for the receptor.

The importance of the hot spot residues detected by CAS can be verified by experimental binding assays of various σ_1 mutants. For instance, in their seminal work Seth et al. clearly demonstrated the obligatory nature of the fully conserved Asp126 and Glu172 for the ligand binding function of the σ_1 receptor via *in vitro* binding assays of the Asp126Gly and Glu172Gly σ_1 mutants to radiolabeled haloperidol.[18] Also, other mutational studies identified Tyr173 as a residue critical for the cholesterol binding activity of the protein.[32]

To summarize all the *in silico* work discussed above, we used MM/PBSA-based simulations and analysis to design and rank 33 compounds for their affinity toward our 3D homology model of the σ_1 receptor. The $K_i(\sigma_1)$ values derived from the MM/PBSA calculations are in agreement (R^2 = 0.84) with those obtained using a 3D pharmacophore model, previously shown to be reliable in reproducing and/or predicting the affinity of similar compounds to the same receptor. Lastly, the combined application of a per residue free energy deconvolution and computational alanine scanning mutagenesis allowed us to dissect the contribution of each single residue belonging to the putative σ_1 receptor binding pocket to ligand binding, yielding fundamental information for further design and development of σ_1 ligands. Furthermore, and perhaps most importantly in the perspective of the present manuscript, those σ_1 residues experimentally found to be involved in ligand binding activity of the receptor were also found critical in our 3D model, according to our PRFEBD and CAS simulations.

SYNTHESIS AND ACTIVITY OF NEW σ_1 LIGANDS AND COMPARISON WITH *IN SILICO* PREDICTIONS

The two series of phenylmethanone (**1a−r**) and amide (**2a−l**) derivatives designed using the molecular modeling method-

dx.doi.org/10.1021/mp300233y | *Mol. Pharmaceutics* 2012, 9, 3107−3126

ology described so far were then synthesized according to the synthetic pathways shown in Scheme 1 (left and right panels, respectively).

Compounds of general formula **1a−r** were prepared following the method depicted in Scheme 1A. Accordingly, the Schiff bases **3a−f** obtained by condensation of 4-(aminomethyl)piperidine with the appropriate aromatic aldehyde (in $CHCl_3/Na_2SO_4$ at room temperature) enabled the selective acylation of the secondary group and afforded the corresponding benzoyl derivatives **4a−f**. Reduction of the imine derivatives **4a−f** with $NaBH_4$ in methanol yielded the corresponding amines **1a−c** and **1j−l**, which, in turn, were alkylated with methyl iodide in EtOH/KOH or with benzyl chloride in acetone (K_2CO_3) to give the tertiary amines **1d−f**, **1m−o**, **1g−i**, and **1p−r**, respectively.

Compounds of the general formula **2a−l** were prepared starting from the Schiff bases **3a−c** (Scheme 1B) obtained by condensation of the appropriate aromatic aldehydes and 4-(aminomethyl)piperidine. The Schiff bases were made to react with benzyl chloride and substituted benzyl chlorides to afford the corresponding imine derivatives **5a−f**. Reduction of **5a−f** with $NaBH_4$ gave the methanamine derivatives **6a−f**. Finally, treatment of compounds **6a−f** with acetyl chloride or benzoyl chloride yielded the corresponding acetamide and benzamide derivatives **2a−l**.

All molecules were subsequently subjected to *in vitro* binding assays, in order to assess their experimental affinity toward the σ_1 receptor (see Tables 5 and 6). The $K_i(\sigma_1)$ values for all 33 compounds were determined using a protocol based on the competitive displacement of [^{3}H]-(+)-pentazocine in a rat liver homogenate preparation.[33,34]

With respect to compounds **1a−r**, the results confirm the presence of a basic nitrogen atom substituted with a small group (H, CH_3) as a fundamental factor to endow the compound with σ_1 affinity. Actually, the N-substitution with a benzyl group decreases the affinity of the derivatives **1g−i** toward the receptor with respect to the corresponding derivatives **1a−f**; contrarily, the presence of a $-CH_3$ group linked to the basic nitrogen atom in compounds **1e** ($K_i(\sigma_1)$ = 30.3 nM) and **1f** ($K_i(\sigma_1)$ = 36.4 nM) improves the σ_1 affinity of this compound. However, the simultaneous absence of a small substituent (e.g., chlorine or methyl group) on the para position of the benzyl moiety decreases the σ_1 receptor affinity of compound **1d** ($K_i(\sigma_1)$ = 75.5 nM) with respect to the corresponding para-substituted compounds **1e** and **1f**. Compound **1e**, characterized by the presence of a chlorine atom on the para position of the benzyl residue and of a methyl group linked to the basic nitrogen atom, explicates the highest σ_1 affinity. The para substitution with chlorine in compound **1b** ($K_i(\sigma_1)$ = 42.3 nM) maintains some level of σ_1 affinity, inferior to that of the corresponding *N*-methyl derivative **1e**, but superior to that of the analogues **1a** ($K_i(\sigma_1)$ = 114 nM) and **1c** ($K_i(\sigma_1)$ = 139 nM). The replacement of the phenyl or substituted phenyl residues in compounds **1j−r** with the pyridine-2-yl, pyridine-3-yl, or pyridine-4yl moieties abolishes the σ_1 affinity of the corresponding compounds. In the derivative series **2a−l**, the amide nitrogen atom is linked to variously substituted benzyl residues and to a 4-methylpiperidin-1-yl spacer, substituted on the benzene ring. The basic nitrogen atom that allows the ionic bond with a receptor acid site belongs to the piperidine cycle. The experimental σ_1 affinity of compound **2c** is rather high ($K_i(\sigma_1)$ = 1.87 nM). Compound **2c** is substituted with chlorine on the para position of the benzyl group linked to piperidine nitrogen atom. The most potent compound of the series, however, is the acetamide derivative **2e**, characterized by a $K_i(\sigma_1)$ value as low as 0.09 nM. Interestingly, the corresponding benzamide derivative **2f** shows a much lower σ_1 receptor affinity ($K_i(\sigma_1)$ = 23.2 nM). Actually, acetamide derivatives are endowed with σ_1 affinity higher than that of corresponding benzamide derivatives, except for compound **2g**. The superior affinity of acetamide derivatives may be attributed to the electron donating effect of the acetamide methyl group that may increase the electronegative character of the carbonyl oxygen and further contribute to the σ_1 binding affinity as hydrogen bond acceptor.

As stated in the introductory paragraphs, one of the main purposes of the entire work was a general validation of our originally proposed 3D model of the σ_1 receptor. Therefore, the direct comparison of the results stemming from the experimental ligand binding assays and the corresponding values predicted by the application of the entire computational ansatz constitutes a fundamental and important point of the entire discussion. Figure 8 illustrates the results of this direct comparison. In detail, Figure 8A shows the remarkable agreement between the affinities for the σ_1 receptor of compounds **1** and **2** predicted by the 3D pharmacophore model ($K_i(\sigma_1)_{3DPh}$) and the corresponding experimental $K_i(\sigma_1)$ values, quantified by a correlation coefficient of 0.89. If this

Table 5. Experimental σ_1 Receptor Affinities ($K_i(\sigma_1)$) and Corresponding Free Energy of Binding Values ($\Delta G_{bind,exp}$) of Compounds 1a−r[a]

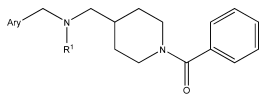

1a-r

compd	Ary	R^1	$K_i(\sigma_1)$ (nM)	$\Delta G_{bind,exp}$ (kcal/mol)[b]
1a	phenyl	H	114 ± 7	−9.47
1b	4-chlorophenyl	H	42.3 ± 5.3	−10.05
1c	4-methylphenyl	H	139 ± 26	−9.35
1d	phenyl	CH_3	75.5 ± 9.7	−9.71
1e	4-chlorophenyl	CH_3	30.3 ± 3.9	−10.25
1f	4-methylphenyl	CH_3	36.4 ± 3.6	−10.14
1g	phenyl	Bz	146 ± 27	−9.32
1h	4-chlorophenyl	Bz	124 ± 24	−9.42
1i	4-methylphenyl	Bz	201 ± 36	−9.13
1j	pyridin-2-yl	H	1664 ± 147	−7.88
1k	pyridin-3-yl	H	1031 ± 95	−8.16
1l	pyridin-4-yl	H	638 ± 24	−8.45
1m	pyridin-2-yl	CH_3	1305 ± 105	−8.02
1n	pyridin-3-yl	CH_3	1578 ± 115	−7.91
1o	pyridin-4-yl	CH_3	1066 ± 130	−8.14
1p	pyridin-2-yl	Bz	506 ± 92	−8.58
1q	pyridin-3-yl	Bz	1401 ± 184	−7.98
1r	pyridin-4-yl	Bz	1020 ± 162	−8.17
(+)-pentazocine			15 ± 3	−10.67
haloperidol			5.7 ± 1	−11.24

[a]The $K_i(\sigma_1)/\Delta G_{bind,exp}$ values for (+)-pentazocine and haloperidol as reference compounds are also reported, for comparison. Errors are given as standard errors of the mean (SEM). [b]The $\Delta G_{bind,exp}$ values were obtained from the corresponding $K_i(\sigma_1)$ values using the relationship $\Delta G_{bind} = -RT \ln(1/K_i)$.

dx.doi.org/10.1021/mp300233y | *Mol. Pharmaceutics* 2012, 9, 3107−3126

Table 6. σ_1 Receptor Affinities of Compounds 2a–l[a]

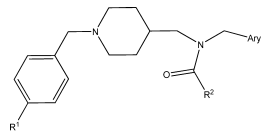

2a-l

compd	Ary	R^1	R^2	$K_i(\sigma_1)$ (nM)	$\Delta G_{bind,exp}$ (kcal/mol)[b]
2a	phenyl	H	CH_3	9.62 ± 1.81	−10.93
2b	phenyl	H	phenyl	18.8 ± 2.2	−10.53
2c	phenyl	Cl	CH_3	1.87 ± 0.29	−11.90
2d	phenyl	Cl	phenyl	24.3 ± 3.6	−10.38
2e	4-chlorophenyl	H	CH_3	0.09 ± 0.03	−13.70
2f	4-chlorophenyl	H	phenyl	23.2 ± 3.2	−10.41
2g	4-chlorophenyl	Cl	CH_3	14.6 ± 1.4	−10.68
2h	4-chlorophenyl	Cl	phenyl	10.7 ± 2.5	−10.87
2i	4-methylphenyl	H	CH_3	14.2 ± 2.5	−10.70
2j	4-methylphenyl	H	phenyl	118 ± 28	−9.45
2k	4-methylphenyl	Cl	CH_3	61.8 ± 7.6	−9.83
2l	4-methylphenyl	Cl	phenyl	66.6 ± 12.5	−9.78
(+)-pentazocine				15 ± 3	−10.67
haloperidol				5.7 ± 1	−11.24

[a]The $K_i(\sigma_1)$ values for (+)-pentazocine and haloperidol as reference compounds are also reported, for comparison. [b]The $\Delta G_{bind,exp}$ values were obtained from the corresponding $K_i(\sigma_1)$ values using the relationship $\Delta G_{bind} = -RT \ln(1/K_i)$.

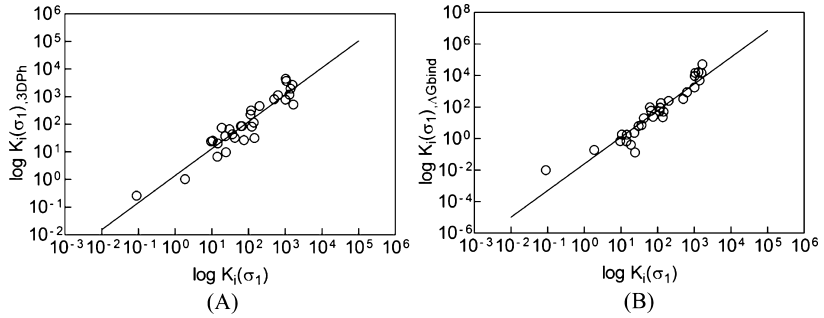

Figure 8. (A) Plot of the experimental vs 3D pharmacophore predicted $K_i(\sigma_1)$ values for the 33 compounds of series **1** and **2** ($R^2 = 0.89$). (B) Plot of the experimental vs MM/PBSA predicted $K_i(\sigma_1)$ values for the 33 compounds of series **1** and **2** ($R^2 = 0.89$).

could be a somewhat expected result, the correlation between the experimental $K_i(\sigma_1)$ values and those derived from the application of the MM/PBSA ranking is even more gratifying: indeed, Figure 8B shows how well the calculated $K_i(\sigma_1)_{\Delta G_{bind}}$ values reproduce the experimental ones ($R^2 = 0.89$), with a correct ranking order. To further confirm the capability of the entire MM/PBSA computational procedure in ranking the affinities of all 33 compounds toward the σ_1 receptor, we compared the values of the ΔG_{bind} calculated by MM/PBSA (Table 2) with those derived from the biological assays (Tables 5 and 6): we can observe that the average unsigned error between these two data sets is 0.93 kcal/mol, and the corresponding root-mean-square deviation is 1.19 kcal/mol. Thus, the remarkable quality of all these correlations, coupled with the correct ranking of the wide range of the σ_1 affinity values, constitutes a further, decisive validation of the putative σ_1 binding site and, overall, of the entire 3D homology model of this intriguingly enigmatic receptor.

CONCLUSIONS

σ receptors were first postulated by Martin et al.[35] based on the actions of SKF 10,047 (*N*-allylnormetazocine) and related benzomorphans. The name "σ" originated from the first letter "S" in SKF 10,047, which was thought to be the prototypic ligand for these binding sites. Unfortunately, SKF 10,047 is now recognized as a nonselective ligand, which contributed to the turbulent early history surrounding these enigmatic receptors. One distinguishing feature of the σ_1 receptor is its promiscuity in binding a wide range of different pharmacological agents, although how binding of these various compounds translates into function(s) through the σ_1 receptor is currently not clear.[34] Since the discovery of the σ_1 receptor, many preclinical studies have implicated the receptor in many important human diseases, from maladies of the central nervous system to cancer, just to name a few. Notwithstanding many pharmacologic responses have been linked to the σ receptors, the function of the σ_1 protein is still a subject of intense study and current debate. Importantly, until very recent times relatively little information regarding the structure of the σ_1 receptor or its ligand binding site was available to the scientific community. Cloning of the σ_1 receptor revealed that the rat brain receptor σ_1 protein consists of 223 amino acids, which results in a molecular weight of 23 kDa. Although human and animal σ_1 receptors show a similarity of more than 95%, unfortunately there is no resemblance of this receptor to other known mammalian proteins.

Lately our group published for the first time a 3D model of the σ_1 receptor protein as obtained from a multistep computational recipe based on homology modeling techniques.[17] The reliability of the proposed σ_1 model and the validity of its putative ligand binding site were assessed by a docking/MMPBSA-based small-scale virtual screening of a series of available σ_1 ligands, and by the receptor model-based design of three new σ_1 ligands, featuring a wide range of activity (from 1.87 to 1578 nM).[17] To definitely confirm the validity of this σ_1 3D model and its reliability as a platform for σ_1-ligand structure-based drug design, in the present work we expanded our study by designing 33 new σ_1 ligands, with affinity for the receptor spanning 5 orders of magnitude. All these compounds were then ranked for receptor affinity by extensive molecular dynamics simulation-based free energy calculations, and the main interactions/receptor residues involved in ligand binding were thoroughly analyzed by applying per residue free energy deconvolution and *in silico* alanine scanning mutagenesis. All compounds were subsequently synthesized in our laboratory and then tested for σ_1 binding activity *in vitro*.

Remarkably, the experimental affinity ranking for all 33 compounds toward the σ_1 receptor was found to be fully consistent with the corresponding predictions obtained from our *in silico* procedure. Therefore, we are convinced that the computational methodology adopted here can be generally employed to estimate the affinity of new σ_1 ligands prior to their synthesis, with an obvious optimization of time and resources. Furthermore, if we reconsider all experimental affinity data listed in Tables 5 and 6, we can see that both sets of compounds **1** and **2** can be classified on the basis of their experimental activity as highly affine ($K_i(\sigma_1) \leq 40.0$ nM, +++), moderately affine ($40.0 < K_i(\sigma_1) < 600$ nM, ++), and poorly affine ($K_i(\sigma_1) \geq 600$ nM, +). According to this classification, and looking at the *in silico* ranking shown it Table 2, we can also conclude that all compounds classified as highly affine (+++) are characterized by ΔG_{bind} values ≤ -11.00 kcal/mol, those with a moderate affinity (++) have $-11.00 < \Delta G_{bind} < -8.50$ kcal/mol, and finally the less affine ones have $\Delta G_{bind} \geq -8.50$ kcal/mol. Taking into account that the entire computational methodology is based on a protein structure obtained via homology modeling techniques, these ranking capacities and the related results ultimately assess the reliability of the σ_1 receptor 3D model in structure-based ligand design.

EXPERIMENTAL SECTION

Computational Details. All compound structures were designed and optimized using *Discovery Studio* (*DS*, v. 2.5, Accelrys Inc., San Diego, CA, USA).[17,19,20] All docking experiments were performed with *Autodock* 4.3,[36] with *Autodock Tools* 1.4.6 on a *win64* platform. A consolidated procedure[23] was used, so it will be reported here only briefly. *DS* was employed to define the size of the binding site, using an opening site of 10 Å and a grid size of 0.7 Å. The dimensions of the *Autodock* grid box, based on the cavity identified by *DS*, was large enough to cover all possible rotations of each ligand. van der Waals interactions and hydrogen bonding (O−H, N−H, and S−H) were modeled with the *Amber* 12-6 and 12-10 Lennard-Jones parameters, respectively, while the distance-dependent relative permittivity of Mehler and Solmajer[37] was applied in the generation of the electrostatic grid maps. 300 Monte Carlo/simulated annealing (MC/SA) runs were performed, with 100 constant temperature cycles for simulated annealing. The GB/SA implicit water model[38] was used in these calculations to mimic the solvated environment. The angles of the side chains and the rotation of the angles φ and ψ were set free during the calculations, while all others parameters of the MC/SA algorithm were kept as default. The structures of all compounds were subjected to cluster analysis with a 1 Å tolerance for an all-atom root-mean-square (RMS) deviation from a lower-energy structure representing each cluster family. The resulting docked conformations were clustered and visualized, and the molecular conformation belonging to the cluster with the lowest (i.e., most favorable) *Autodock* energy was selected to carry for further modeling.

Each ligand/receptor complex obtained from the docking procedure was further refined in *Amber* 11[39] using the quenched molecular dynamics (QMD) method.[23,40] Atomic charges were derived by the AM1-BCC method,[41] while the force fields *ff03*[42] and the general *Amber* force field (*gaff*)[43] were used to parametrize the σ_1 receptor and all compounds, respectively. According to the QMD, 1 ns molecular dynamics (MD) simulation at 300 K was employed to sample the conformational space of each ligand−receptor complex in the GB/SA continuum solvation environment.[25] The integration step was equal to 1 fs. After each picosecond, each system was cooled to 0 K, and the structure was extensively minimized and stored. To prevent global conformational changes of the protein, the backbone atoms of the protein binding site were constrained by a harmonic force constant of 100 kcal/Å, whereas the amino acid side chains and the ligands were allowed moving without any constraint. The best energy configuration of each complex resulting from the previous step was subsequently solvated by a cubic box of TIP3P[44] water molecules extending at least 10 Å in each direction from the solute. The system was then neutralized with the addition of 21 Na^+ and 15 Cl^- counterions; further, the solution ionic strength was adjusted to the physiological value of 0.15 M by adding the required amounts of Na^+ and Cl^- ions.

Each solvated system was relaxed by 500 steps of steepest descent followed by another 500 conjugate-gradient minimization steps, and then gradually heated to a temperature of 300 K in intervals of 50 ps of NVT MD, using a Verlet integration time step of 1.0 fs. The Langevin thermostat was used to control temperature, with a collision frequency of 2.0 ps^{-1}. The *SHAKE* method[45] was used to constrain all of the covalent bonds involving hydrogen atoms, while long-range nonbonded van der Waals interactions were truncated by using a dual cutoff of 6 and 12 Å, respectively. The particle mesh Ewald (PME) method[46] was applied to treat long-range electrostatics interactions. The protein was restrained with a force constant of 2.0 kcal $(mol\ Å)^{-1}$, and all simulations were carried out with periodic boundary conditions.

The density of each system was subsequently equilibrated via MD runs in the isothermal−isobaric (NPT) ensemble, with isotropic position scaling and a pressure relaxation time of 1.0 ps, for 50 ps with a time step of 1 fs. All restraints on the protein atoms were then removed, and each system was further equilibrated using NPT MD runs at 300 K, with a pressure relaxation time of 2.0 ps. Three equilibration steps were performed, each 2 ns long and with a time step of 2.0 fs. To check the system stability, the fluctuations of the root-mean-square deviation (RMSD) of the simulated position of the backbone atoms of the σ_1 receptor with respect to those of the initial protein were monitored. All chemicophysical parameters and RMSD values showed very low fluctuations at the end of the equilibration process (see Figure SI1 in the available

Supporting Information), indicating that the systems reached a true equilibrium condition.

Each equilibration phase was followed by a data production run consisting of 4 ns of MD simulations in the canonical (constant volume−constant temperature, NVT) ensemble. Only the last 2 ns of each equilibrated MD trajectory were considered for statistical data collections. A total of 100 trajectory snapshots were analyzed for each drug/receptor complex.

The binding free energy, ΔG_{bind}, between each ligand and the σ_1 receptor was estimated resorting to the MM/PBSA (molecular mechanics/Poisson−Boltzmann surface area) approach.[21] According to this well-validated methodology,[17,23,24] the binding free energy between a drug and its protein target in a solvent was obtained as the sum of the interaction energy between the receptor and the ligand (ΔE_{MM}), the solvation free energy (ΔG_{sol}), and the conformational entropy contribution ($-T\Delta S$), averaged over a series of snapshots from the corresponding MD trajectories:

$$\Delta G_{bind} = \Delta E_{MM} + \Delta G_{sol} - T\Delta S \quad (1)$$

The ΔE_{MM} term in eq 1 was obtained directly from the molecular mechanics interaction energies as

$$\Delta E_{MM} = \Delta E_{vdW} + \Delta E_{ele} \quad (2)$$

where ΔE_{vdW} and ΔE_{ele} are the van der Waals and electrostatic components of the nonbonded interaction energy, respectively.

The second term in eq 1, the solvation energy ΔG_{sol}, can also be partitioned into two different contributions:

$$\Delta G_{sol} = \Delta G_{PB} + \Delta G_{np} \quad (3)$$

In this work, the polar term of ΔG_{sol}, ΔG_{PB}, was estimated using *DelPhi*,[47] which solves the Poisson−Boltzmann equations numerically and calculates the electrostatic energy according to the electrostatic potential. In these calculations, the interior and exterior dielectric constant values were set equal to 1 and 80, respectively. A grid spacing of 0.5 per Å, extending 20% beyond the dimensions of the solute, was employed. The value of the nonpolar component of ΔG_{sol}, ΔG_{np}, was calculated using the following relationship:[48]

$$\Delta G_{np} = \gamma \times SA + \beta \quad (4)$$

in which γ = 0.00542 kcal (mol Å^2)$^{-1}$, β = 0.92 kcal/mol, and SA is the molecular surface area estimated by means of the MSMS software.[49]

The change in solute entropy upon association ($-T\Delta S$ in eq 1) was evaluated through normal-node analysis[50] using the *Nmode* module of *AMBER 11*. In the first step of this calculation, an 8 Å sphere around the ligand was cut out from an MD snapshot for each ligand−protein complex. This value was shown to be large enough to yield converged mean changes in solute entropy. On the basis of the size-reduced snapshots of the complex, we generated structures of the uncomplexed reactants by removing the atoms of the protein and ligand, respectively. Each of those structures was minimized, using a distance-dependent dielectric constant $\varepsilon = 4r$, to account for solvent screening, and its entropy was calculated using classical statistical formulas and normal mode analysis. To minimize the effects due to different conformations adopted by individual snapshots we averaged the estimation of entropy over 40 snapshots.

Two further computational techniques were employed to validate and confirm the reliability of the proposed binding site of σ_1 receptor. First, a per residue binding free energy decomposition (PRBFED) was performed exploiting the MD trajectory of each given compound/receptor complex, with the aim of identifying the key residues involved in the ligand−receptor interaction. This analysis was carried out using the MM/GBSA approach[29,51] and was based on the same snapshots used in the binding free energy calculation. Notably, this approach allows quantification of not only the contributions afforded by the side chain of the involved residues to drug binding but also those arising from the protein backbone atoms.[52]

The role of the key residues identified by PRBFED was further studied by performing computational alanine scanning (CAS) experiments.[53] Accordingly, the absolute binding free energy of each mutant receptor, in which one of the key residues was replaced with alanine, was calculated with the MM/PBSA method. The difference in the binding free energy between the wild-type (wt) σ_1 receptor and its alanine mutant (mut) counterpart, $\Delta\Delta G_{bind}$, is as follows:

$$\Delta\Delta G_{bind} = \Delta G_{bind,wt} - \Delta G_{bind,mut} \quad (5)$$

Thus, the CAS methodology allows estimation of the contribution of a given residue with respect to the overall ligand−receptor binding free energy;[42] indeed, according to eq 5, a negative value of $\Delta\Delta G_{bind}$ indicated a favorable contribution for the wild type residue in that position and *vice versa*.

Each σ_1 alanine mutant structure was generated by truncating the mutated residue at the C_γ atom, and replacing it with a hydrogen. As suggested by Moreira and colleagues,[54] to calculate the binding free energy of the mutant structures and their ligands the single trajectory protocol was carried on exploiting the corresponding wt protein MD simulation.

All MD simulations were carried out using the *Sander* and *Pmemd* modules of *AMBER 11*, running in parallel on 256 processors of the IBM/SP6 calculation cluster of the CINECA supercomputer facility (Bologna, Italy). The entire computational procedure was optimized by integrating *AMBER 11* in *modeFRONTIER*, a multidisciplinary and multiobjective optimization and design environment.[55]

Synthesis of New σ_1 Ligands. General. Unless otherwise noted, starting materials and reagents were obtained from commercial suppliers and used without purification. Melting points were determined with a Buchi 510 capillary apparatus and are uncorrected. Infrared spectra in Nujol mulls were recorded on a JaskoFT200 spectrophotometer. Proton nuclear magnetic resonance (^{1}H NMR) spectra were determined on a Varian Gemini 200 spectrometer, and the chemical shifts are reported as δ (ppm) in $CDCl_3$ solution. Coupling constants J are expressed in hertz (Hz). Reaction courses and product mixtures were routinely monitored by thin-layer chromatography (TLC) on silica gel precoated F254 Merck plates. ESI-MS spectra were obtained on a PE-API I spectrometer by infusion of a solution of the sample in MeOH. Elemental analyses (C, H, N) were performed on a Carlo Erba 1106 analyzer and were within ±0.3 of the theoretical value (see Table SI1 in the Supporting Information).

***N*-Benzylidene-1-(piperidin-4-yl)methanamine (3a).** Na_2SO_4 (0.33 g, 2.32 mmol) was added to a mixture of 4-(aminomethyl)piperidine (0.25 g, 2.19 mmol) and benzaldehyde (0.23 g, 2.19 mmol) in 100 mL of $CHCl_3$ under stirring at

room temperature. After 24 h, the solution was filtered to remove the inorganic salt. The organic phase was concentrated *in vacuo* to give compound **3a** as a solid; mp 140−142 °C, yield 0.42 g (96%). IR cm^{-1} (Nujol): 1692, 3389 cm^{-1}. ^1H NMR ($CDCl_3$−TMS) ppm (δ): 1.61−1.84 (m, 6H, $H_{3,3'}$-$H_{5,5'}$-H_4, pip. + N*H* disappearing on deuteration); 2.62 (m, 2H, H_2-H_6, pip.); 3.09 (m, 2H, $H_{2'}$-$H_{6'}$, pip.); 3.48 (d, 2H, CH_2); 7.36−7.69 (m, 5H, arom.); 8.20 (s, 1H, N=C*H*−Ar). MS: *m*/*z* 203 [MH^+].

Compounds **3b−f** were synthesized following the same procedure, starting from the appropriate substituted aldehyde.

***N*-(4-Chlorobenzylidene)-1-(piperidin-4-yl)-methanamine (3b).** IR cm^{-1} (Nujol): 1690, 3393 cm^{-1}. ^1H NMR ($CDCl_3$−TMS) ppm (δ): 1.60−1.89 (m, 6H, $H_{3,3'}$-$H_{5,5'}$-H_4, pip. + N*H* disappearing on deuteration); 2.65 (m, 2H, H_2-H_6, pip.); 3.15 (m, 2H, $H_{2'}$-$H_{6'}$, pip.); 3.46 (d, 2H, CH_2); 7.30−7.70 (m, 4H, arom.); 8.22 (s, 1H, N=C*H*−Ar). MS: *m*/*z* 237 [MH^+], 239 [MH^+ + 2].

***N*-(4-Methylbenzylidene)-1-(piperidin-4-yl)-methanamine (3c).** IR cm^{-1} (Nujol): 1689, 3382 cm^{-1}. ^1H NMR ($CDCl_3$−TMS) ppm (δ): 1.55−1.83 (m, 6H, $H_{3,3'}$-$H_{5,5'}$-H_4, pip. + N*H* disappearing on deuteration); 2.32 (s, 3H, CH_3); 2.69 (m, 2H, H_2-H_6, pip.); 3.06 (m, 2H, $H_{2'}$-$H_{6'}$, pip.); 3.40 (d, 2H, CH_2); 7.22−7.69 (m, 4H, arom.); 8.19 (s, 1H, N=C*H*−Ar). MS: *m*/*z* 217 [MH^+].

***N*-(Pyridin-2-ylmethylen)-1-(piperidin-4-yl)-methanamine (3d).** IR cm^{-1} (Nujol): 1691, 3393 cm^{-1}. ^1H NMR ($CDCl_3$−TMS) ppm (δ): 1.35−1.93 (m, 5H, $H_{3,3'}$-$H_{5,5'}$-H_4, pip.); 2.28 (large spectrum, 1H, N*H* disappearing on deuteration); 2.73 (m, 2H, H_2-H_6, pip.); 3.12 (m, 2H, $H_{2'}$-$H_{6'}$, pip.); 3.56 (d, 2H, CH_2); 7.28−7.80 (m, 3H, arom.); 8.34 (s, 1H, N=C*H*−Ar); 8.64 (m, 1H, arom.). MS: *m*/*z* 204 [MH^+].

***N*-(Pyridin-3-ylmethylen)-1-(piperidin-4-yl)-methanamine (3e).** IR cm^{-1} (Nujol): 1680, 3387 cm^{-1}. ^1H NMR ($CDCl_3$−TMS) ppm (δ): 1.39−1.95 (m, 5H, $H_{3,3'}$-$H_{5,5'}$-H_4, pip.); 2.30 (large spectrum, 1H, N*H* disappearing on deuteration); 2.71 (m, 2H, H_2-H_6, pip.); 3.10 (m, 2H, $H_{2'}$-$H_{6'}$, pip.); 3.52 (d, 2H, CH_2); 7.36−7.92 (m, 3H, arom.); 8.30 (s, 1H, N=C*H*−Ar); 8.86 (m, 1H, arom.). MS: *m*/*z* 204 [MH^+].

***N*-(Pyridin-4-ylmethylen)-1-(piperidin-4-yl)-methanamine (3f).** IR cm^{-1} (Nujol): 1685, 3392 cm^{-1}. ^1H NMR ($CDCl_3$−TMS) ppm (δ): 1.34−1.86 (m, 5H, $H_{3,3'}$-$H_{5,5'}$-H_4, pip.); 2.25 (large spectrum, 1H, N*H* disappearing on deuteration); 2.75 (m, 2H, H_2-H_6, pip.); 3.15 (m, 2H, $H_{2'}$-$H_{6'}$, pip.); 3.61 (d, 2H, CH_2); 7.86 (m, 2H, arom.); 8.30 (s, 1H, N=C*H*−Ar); 8.60 (m, 2H, arom.). MS: *m*/*z* 204 [MH^+].

(4-((Benzylideneamino)methyl)piperidin-1-yl)-(phenyl)methanone (4a). A solution of benzoyl chloride (0.26 g, 1.87 mmol) in 5 mL of THF was added dropwise at 0 °C to a mixture of **3a** (0.44 g, 1.87 mmol) and triethylamine (0.23 g, 2.28 mmol) in 10 mL of THF. After 4 h, the solution was concentrated under reduced pressure and $CHCl_3$ (30 mL) was added. The organic phase was washed with distilled water (3 × 15 mL), dried with Na_2SO_4, and concentrated *in vacuo* to obtain **4a** as a pure oil; yield 0.51 g (80%). IR cm^{-1} (Nujol): 1645, 1718 cm^{-1}. ^1H NMR ($CDCl_3$−TMS) ppm (δ): 1.58−1.92 (m, 5H, $H_{3,3'}$-$H_{5,5'}$-H_4, pip.); 2.98−3.21 (m, 4H, $H_{2,2'}$-$H_{6,6'}$, pip.) ; 3.58 (d, 2H, CH_2); 7.38−8.06 (m, 9H, arom.); 8.25 (s, 1H, N=C*H*−Ar). MS: *m*/*z* 341 [MH^+], 343 [MH^+ + 2].

Compounds **4b−f** were obtained following the same approach, starting from **3b−f**.

(4-((4-Chlorobenzylideneamino)methyl)piperidin-1-yl)(phenyl)methanone (4b). IR cm^{-1} (Nujol): 1645, 1718 cm^{-1}. ^1H NMR ($CDCl_3$−TMS) ppm (δ): 1.58−1.92 (m, 5H, $H_{3,3'}$-$H_{5,5'}$-H_4, pip.); 2.98−3.21 (m, 4H, $H_{2,2'}$-$H_{6,6'}$, pip.) ; 3.58 (d, 2H, CH_2); 7.38−8.06 (m, 9H, arom.); 8.25 (s, 1H, N=C*H*−Ar). MS: *m*/*z* 341 [MH^+], 343 [MH^+ + 2].

(4-((4-Methylbenzylideneamino)methyl)piperidin-1-yl)(phenyl)methanone (4c). IR cm^{-1} (Nujol): 1641, 1716 cm^{-1}. ^1H NMR ($CDCl_3$−TMS) ppm (δ): 1.50−1.97 (m, 5H, $H_{3,3'}$-$H_{5,5'}$-H_4, pip.); 2.32 (s, 3H, CH_3); 2.90−3.15 (m, 4H, $H_{2,2'}$-$H_{6,6'}$, pip.) ; 3.42 (d, 2H, CH_2); 7.30−7.97 (m, 9H, arom.); 8.16 (s, 1H, N=C*H*−Ar). MS: *m*/*z* 321 [MH^+].

Phenyl(4-((pyridin-2-ylmethylenamino)methyl)-piperidin-1-yl)methanone (4d). IR cm^{-1} (Nujol): 1651, 1720 cm^{-1}. ^1H NMR ($CDCl_3$−TMS) ppm (δ): 1.53−2.00 (m, 5H, $H_{3,3'}$-$H_{5,5'}$-H_4, pip.); 2.82−3.12 (m, 4H, $H_{2,2'}$-$H_{6,6'}$, pip.) ; 3.53 (d, 2H, CH_2);); 7.28−7.91 (m, 8H, arom.); 8.32 (s, 1H, N=C*H*−Ar); 8.65 (m, 1H, arom.). MS: *m*/*z* 308 [MH^+].

Phenyl(4-((pyridin-3-ylmethylenamino)methyl)-piperidin-1-yl)methanone (4e). IR cm^{-1} (Nujol): 1650, 1718 cm^{-1}. ^1H NMR ($CDCl_3$−TMS) ppm (δ): 1.51−1.99 (m, 5H, $H_{3,3'}$-$H_{5,5'}$-H_4, pip.); 2.81−3.08 (m, 4H, $H_{2,2'}$-$H_{6,6'}$, pip.) ; 3.52 (d, 2H, CH_2);); 7.28−8.04 (m, 8H, arom.); 8.11 (s, 1H, N=C*H*−Ar); 8.60 (m, 1H, arom.). MS: *m*/*z* 308 [MH^+].

Phenyl(4-((pyridin-4-ylmethylenamino)methyl)-piperidin-1-yl)methanone (4f). IR cm^{-1} (Nujol): 1653, 1722 cm^{-1}. ^1H NMR ($CDCl_3$−TMS) ppm (δ): 1.53−2.00 (m, 5H, $H_{3,3'}$-$H_{5,5'}$-H_4, pip.); 2.82−3.12 (m, 4H, $H_{2,2'}$-$H_{6,6'}$, pip.); 3.53 (d, 2H, CH_2); 7.31−8.05 (m, 7H, arom.); 8.17 (s, 1H, N=C*H*−Ar); 8.70 (m, 2H, arom.).

(4-((Benzylamino)methyl)piperidin-1-yl)(phenyl)-methanone (1a). $NaBH_4$ (0.13 g, 3.47 mmol) was slowly added to a mixture of **4a** (0.58 g, 1.69 mmol) in 25 mL of MeOH. After stirring overnight, the solution was concentrated *in vacuo* and extracted with AcOEt (30 mL). The organic phase was washed with distilled water (3 × 15 mL) and then evaporated under reduced pressure, yielding **1a** as a pure and colorless oil; yield 0.38 g (69%). IR cm^{-1} (Nujol): 1723, 3258 cm^{-1}. ^1H NMR ($CDCl_3$−TMS) ppm (δ): 1.28−1.72 (m, 5H, $H_{3,3'}$-$H_{5,5'}$-H_4, pip.); 2.01 (s broad, 1H, N*H* disappearing on deuteration); 2.52 (d, 2H, CH_2); 2.80−2.99 (m, 4H, $H_{2,2'}$-$H_{6,6'}$, pip.); 3.77 (s, 2H, N−CH_2−aryl) 7.25−7.41 (m, 9H, arom.). MS: *m*/*z* 343 [MH^+], 345 [MH^+ + 2].

Compounds **1b−c** and **1j−l** were synthesized according to the same procedure, starting from the respective intermediates.

(4-((4-Chlorobenzylamino)methyl)piperidin-1-yl)-(phenyl)methanone (1b). IR cm^{-1} (Nujol): 1723, 3258 cm^{-1}. ^1H NMR ($CDCl_3$−TMS) ppm (δ): 1.28−1.72 (m, 5H, $H_{3,3'}$-$H_{5,5'}$-H_4, pip.); 2.01 (large spectrum, 1H, N*H* disappearing on deuteration); 2.52 (d, 2H, CH_2); 2.80−2.99 (m, 4H, $H_{2,2'}$-$H_{6,6'}$, pip.); 3.77 (s, 2H, N−CH_2−aryl) 7.25−7.41 (m, 9H, arom.). MS: *m*/*z* 343 [MH^+], 345 [MH^+ + 2].

(4-((4-Methylbenzylamino)methyl)piperidin-1-yl)-(phenyl)methanone (1c). IR cm^{-1} (Nujol): 1722, 3250 cm^{-1}. ^1H NMR ($CDCl_3$−TMS) ppm (δ): 1.26−1.69 (m, 5H, $H_{3,3'}$-$H_{5,5'}$-H_4, pip.); 2.05 (large spectrum, 1H, N*H* disappearing on deuteration); 2.33 (s, 3H, CH_3); 2.40 (d, 2H, CH_2); 2.79−3.01 (m, 4H, $H_{2,2'}$-$H_{6,6'}$, pip.); 3.43 (s, 2H, N−CH_2−aryl) 7.14−7.39 (m, 9H, arom.). MS: *m*/*z* 323 [MH^+].

(4-((Pyridin-2-ylmethylamino)methyl)piperidin-1-yl)-(phenyl)methanone (1j). IR cm^{-1} (Nujol): 1720, 3261 cm^{-1}. ^1H NMR ($CDCl_3$−TMS) ppm (δ): 1.23−1.54 (m, 5H, $H_{3,3'}$-$H_{5,5'}$-H_4, pip.); 2.05 (large spectrum, 1H, N*H* disappearing on deuteration); 2.59 (d, 2H, CH_2); 2.63−3.02 (m, 4H, $H_{2,2'}$-$H_{6,6'}$,

dx.doi.org/10.1021/mp300233y | *Mol. Pharmaceutics* 2012, 9, 3107−3126

pip.); 3.90 (s, 2H, N−CH_2−aryl) 7.27−7.65 (m, 8H, arom.); 8.55 (m, 1H, arom.). MS: *m/z* 310 [MH^+].

(4-((Pyridin-3-ylmethylamino)methyl)piperidin-1-yl)-(phenyl)methanone (1k). IR cm^{-1} (Nujol): 1719, 3265 cm^{-1}. ^1H NMR ($CDCl_3$−TMS) ppm (δ): 1.26−1.60 (m, 5H, $H_{3,3'}$-$H_{5,5'}$-H_4, pip.); 1.85 (large spectrum, 1H, N*H* disappearing on deuteration); 2.58 (d, 2H, CH_2); 2.69−3.04 (m, 4H, $H_{2,2'}$-$H_{6,6'}$, pip.); 3.81 (s, 2H, N−CH_2−aryl) 7.27−7.78 (m, 8H, arom.); 8.52 (m, 1H, arom.). MS: *m/z* 310 [MH^+].

(4-((Pyridin-4-ylmethylamino)methyl)piperidin-1-yl)-(phenyl)methanone (1l). IR cm^{-1} (Nujol): 1722, 3266 cm^{-1}. ^1H NMR ($CDCl_3$−TMS) ppm (δ): 1.20−1.51 (m, 5H, $H_{3,3'}$-$H_{5,5'}$-H_4, pip.); 1.89 (large spectrum, 1H, N*H* disappearing on deuteration); 2.64 (d, 2H, CH_2); 2.70−3.01 (m, 4H, $H_{2,2'}$-$H_{6,6'}$, pip.); 3.49 (s, 2H, N−CH_2−aryl) 7.27−7.48 (m, 8H, arom.); 8.61 (m, 1H, arom.). MS: *m/z* 310 [MH^+].

(4-((Benzyl(methyl)amino)methyl)piperidin-1-yl)-(phenyl)methanone (1d). Compound **1a** (0.18 g, 0.61 mmol) was dissolved in 10 mL of EtOH; KOH (0.07 g, 1.22 mmol) and CH_3I (0.09 g, 0.61 mmol) were then added. The reaction mixture was heated at reflux temperature, and the reaction was carried out with stirring. After 6 h, EtOH was evaporated under reduced pressure and the crude residue was extracted with $CHCl_3$ (20 mL). The organic phase was washed with distilled water (3 × 10 mL), dried with Na_2SO_4, and concentrated *in vacuo*, giving **1d** as a pure pale oil; yield 0.20 g (76%). IR cm^{-1} (Nujol): 1719 cm^{-1}. ^1H NMR ($CDCl_3$−TMS) ppm (δ): 1.20−1.65 (m, 5H, $H_{3,3'}$-$H_{5,5'}$-H_4, pip.); 2.19 (d, 2H, CH_2); 2.23 (s, 3H, CH_3); 2.80−3.01 (m, 4H, $H_{2,2'}$-$H_{6,6'}$, pip.); 3.79 (s, 2H, N−CH_2−aryl) 7.27−7.50 (m, 10H, arom.). MS: *m/z* 323 [MH^+].

Compounds **1e−f** and **1m−o** were obtained following the same synthetic pathway, starting from the respective intermediates.

(4-(((4-Chlorobenzyl)(methyl)amino)methyl)-piperidin-1-yl)(phenyl)methanone (1e). IR cm^{-1} (Nujol): 1722 cm^{-1}. ^1H NMR ($CDCl_3$−TMS) ppm (δ): 1.26−1.80 (m, 5H, $H_{3,3'}$-$H_{5,5'}$-H_4, pip.); 2.17 (d, 2H, CH_2); 2.22 (s, 3H, CH_3); 2.71−3.02 (m, 4H, $H_{2,2'}$-$H_{6,6'}$, pip.); 3.75 (s, 2H, N−CH_2−aryl) 7.26−7.49 (m, 9H, arom.). MS: *m/z* 357 [MH^+], 359 [MH^+ + 2].

(4-(((4-Methylbenzyl)(methyl)amino)methyl)-piperidin-1-yl)(phenyl)methanone (1f). IR cm^{-1} (Nujol): 1720 cm^{-1}. ^1H NMR ($CDCl_3$−TMS) ppm (δ): 1.27−1.68 (m, 5H, $H_{3,3'}$-$H_{5,5'}$-H_4, pip.); 2.18 (d, 2H, CH_2); 2.23 (s, 3H, CH_3); 2.33 (s, 3H, Ph−CH_3); 2.69−2.97 (m, 4H, $H_{2,2'}$-$H_{6,6'}$, pip.); 3.79 (s, 2H, N−CH_2−aryl) 7.18−7.51 (m, 9H, arom.). MS: *m/z* 337 [MH^+].

(4-((Methyl(pyridin-2-ylmethyl)amino)methyl)-piperidin-1-yl)(phenyl)methanone (1m). IR cm^{-1} (Nujol): 1718 cm^{-1}. ^1H NMR ($CDCl_3$−TMS) ppm (δ): 1.25−1.72 (m, 5H, $H_{3,3'}$-$H_{5,5'}$-H_4, pip.); 2.20 (d, 2H, CH_2); 2.25 (s, 3H, CH_3); 2.70−3.00 (m, 4H, $H_{2,2'}$-$H_{6,6'}$, pip.); 3.64 (s, 2H, N−CH_2−aryl) 7.26−7.80 (m, 8H, arom.); 8.51 (m, 1H, arom.). MS: *m/z* 324 [MH^+].

(4-((Methyl(pyridin-3-ylmethyl)amino)methyl)-piperidin-1-yl)(phenyl)methanone (1n). IR cm^{-1} (Nujol): 1723 cm^{-1}. ^1H NMR ($CDCl_3$−TMS) ppm (δ): 1.28−1.81 (m, 5H, $H_{3,3'}$-$H_{5,5'}$-H_4, pip.); 2.19 (d, 2H, CH_2); 2.23 (s, 3H, CH_3); 2.72−3.05 (m, 4H, $H_{2,2'}$-$H_{6,6'}$, pip.); 3.49 (s, 2H, N−CH_2−aryl) 7.27−7.75 (m, 8H, arom.); 8.58 (m, 1H, arom.). MS: *m/z* 324 [MH^+].

(4-((Methyl(pyridin-4-ylmethyl)amino)methyl)-piperidin-1-yl)(phenyl)methanone (1o). IR cm^{-1} (Nujol): 1723 cm^{-1}. ^1H NMR ($CDCl_3$−TMS) ppm (δ): 1.28−1.80 (m, 5H, $H_{3,3'}$-$H_{5,5'}$-H_4, pip.); 2.18 (d, 2H, CH_2); 2.24 (s, 3H, CH_3); 2.78−3.10 (m, 4H, $H_{2,2'}$-$H_{6,6'}$, pip.); 3.48 (s, 2H, N−CH_2−aryl) 7.25−7.83 (m, 8H, arom.); 8.55 (m, 1H, arom.). MS: *m/z* 324 [MH^+].

(4-((Dibenzylamino)methyl)piperidin-1-yl)(phenyl)-methanone (1g). Compound **1a** (0.25 g, 0.85 mmol) was dissolved in 25 mL of acetone with K_2CO_3 (0.23 g, 1.70 mmol) and benzyl chloride (0.13 g, 1.02 mmol). The reaction mixture was heated at reflux temperature, and the reaction was carried out with stirring. After 8 h, the solution was filtered and the solvent removed. The organic phase (AcOEt) was washed with distilled water, and subsequently the solvent was evaporated to obtain **1g** as pure pale oil; yield 0.19 g (56%). IR cm^{-1} (Nujol): 1716 cm^{-1}. ^1H NMR ($CDCl_3$−TMS) ppm (δ): 1.18−1.76 (m, 5H, $H_{3,3'}$-$H_{5,5'}$-H_4, pip.); 2.29 (d, 2H, CH_2); 2.85−3.08 (m, 4H, $H_{2,2'}$-$H_{6,6'}$, pip.); 3.80 (s, 4H, N−CH_2−aryl); 7.28−7.86 (m, 15H, arom.). MS: *m/z* 399 [MH^+].

Compounds **1h−i** and **1p−r** were obtained by the same procedure, starting from the relevant intermediates.

(4-((Benzyl(4-chlorobenzyl)amino)methyl)(phenyl)-methanone (1h). IR cm^{-1} (Nujol): 1721 cm^{-1}. ^1H NMR ($CDCl_3$−TMS) ppm (δ): 1.26−1.81 (m, 5H, $H_{3,3'}$-$H_{5,5'}$-H_4, pip.); 2.53 (d, 2H, CH_2); 2.80−3.01 (m, 4H, $H_{2,2'}$-$H_{6,6'}$, pip.); 3.81 (s, 4H, N−CH_2−aryl); 7.22−7.87 (m, 14H, arom.). MS: *m/z* 433 [MH^+], 435 [MH^+ + 2].

(4-((Benzyl(4-methylbenzyl)amino)methyl)(phenyl)-methanone (1i). IR cm^{-1} (Nujol): 1722 cm^{-1}. ^1H NMR ($CDCl_3$−TMS) ppm (δ): 1.30−1.75 (m, 5H, $H_{3,3'}$-$H_{5,5'}$-H_4, pip.); 2.34 (s, 3H, CH_3); 2.43 (d, 2H, CH_2); 2.89−3.12 (m, 4H, $H_{2,2'}$-$H_{6,6'}$, pip.); 3.72 (s, 4H, N−CH_2−aryl); 7.30−7.81 (m, 14H, arom.). MS: *m/z* 413 [MH^+].

(4-((Benzyl(pyridin-2-ylmethyl)amino)methyl)-piperidin-1-yl)(phenyl)methanone (1p). IR cm^{-1} (Nujol): 1723 cm^{-1}. ^1H NMR ($CDCl_3$−TMS) ppm (δ): 1.22−1.81 (m, 5H, $H_{3,3'}$-$H_{5,5'}$-H_4, pip.); 2.27 (d, 2H, CH_2); 2.78−3.02 (m, 4H, $H_{2,2'}$-$H_{6,6'}$, pip.); 3.63 (s, 2H, N−CH_2−phenyl); 3.74 (s, 2H, N−CH_2−pyridine); 7.28−7.78 (m, 13H, arom.); 8.55 (m, 1H, arom.). MS: *m/z* 400 [MH^+].

(4-((Benzyl(pyridin-3-ylmethyl)amino)methyl)-piperidin-1-yl)(phenyl)methanone (1q). IR cm^{-1} (Nujol): 1720 cm^{-1}. ^1H NMR ($CDCl_3$−TMS) ppm (δ): 1.23−1.79 (m, 5H, $H_{3,3'}$-$H_{5,5'}$-H_4, pip.); 2.31 (d, 2H, CH_2); 2.76−3.00 (m, 4H, $H_{2,2'}$-$H_{6,6'}$, pip.); 3.56 (s, 2H, N−CH_2−phenyl); 3.81 (s, 2H, N−CH_2−pyridine); 7.27−7.83 (m, 13H, arom.); 8.56 (m, 1H, arom.). MS: *m/z* 400 [MH^+].

(4-((Benzyl(pyridin-4-ylmethyl)amino)methyl)-piperidin-1-yl)(phenyl)methanone (1r). IR cm^{-1} (Nujol): 1725 cm^{-1}. ^1H NMR ($CDCl_3$−TMS) ppm (δ): 1.27−1.82 (m, 5H, $H_{3,3'}$-$H_{5,5'}$-H_4, pip.); 2.30 (d, 2H, CH_2); 2.75−3.07 (m, 4H, $H_{2,2'}$-$H_{6,6'}$, pip.); 3.58 (s, 2H, N−CH_2−phenyl); 3.80 (s, 2H, N−CH_2−pyridine); 7.25−7.91 (m, 13H, arom.); 8.58 (m, 1H, arom.). MS: *m/z* 400 [MH^+].

***N*-Benzylidene-1-(1-benzylpiperidin-4-yl)-methanamine (5a).** A solution of benzyl chloride (0.25 g, 2.01 mmol) in 5 mL of acetone was added to a mixture of **3a** (0.40 g, 2.01 mmol) and K_2CO_3 (0.33 g, 2.41 mmol) in 20 mL of acetone. After 4 h, the solution was filtered and the solvent was removed at reduced pressure. The crude residue was extracted with $CHCl_3$ (50 mL) and washed with distilled water (3 × 15 mL). The organic phase was dried with Na_2SO_4 and

concentrated *in vacuo*, giving **5a** as a pure yellow oil; yield 0.48 g (82%). IR cm^{-1} (Nujol): 1640. ^1H NMR ($CDCl_3$–TMS) ppm (δ): 1.63–2.02 (m, 5H, $H_{3,3'}$-$H_{5,5'}$-H_4, pip.); 2.15–2.26 (m, 2H, H_2-H_6, pip.); 2.83–3.06 (m, 2H, $H_{2'}$-$H_{6'}$, pip.) 3.48 (d, 2H, CH_2); 3.60 (s, 2H, N–CH_2–phenyl); 7.22–7.74 (m, 10H, arom.); 8.23 (s, 1H, N=C*H*–Ar). MS: *m*/*z* 293 [MH^+].

Derivatives **5b–f** were obtained by the same synthetic route starting from the appropriate Schiff bases **3a–c** and benzyl chloride or 4-chlorobenzyl chloride, respectively.

***N*-Benzylidene-1-(1-(4-chlorobenzyl)piperidin-4-yl)-methanamine (5b).** IR cm^{-1} (Nujol): 1640. ^1H NMR ($CDCl_3$–TMS) ppm (δ): 1.58–1.99 (m, 5H, $H_{3,3'}$-$H_{5,5'}$-H_4, pip.); 2.16–2.28 (m, 2H, H_2-H_6, pip.); 2.81–3.02 (m, 2H, $H_{2'}$-$H_{6'}$, pip.) 3.46 (d, 2H, CH_2); 3.63 (s, 2H, N–CH_2–phenyl); 7.25–7.79 (m, 9H, arom.); 8.27 (s, 1H, N=C*H*–Ar). MS: *m*/*z* 327 [MH^+], 328 [MH^+ + 2].

***N*-(4-Chlorobenzylidene)-1-(1-benzylpiperidin-4-yl)-methanamine (5c).** IR cm^{-1} (Nujol): 1636. ^1H NMR ($CDCl_3$–TMS) ppm (δ): 1.61–2.04 (m, 5H, $H_{3,3'}$-$H_{5,5'}$-H_4, pip.); 2.19–2.31 (m, 2H, H_2-H_6, pip.); 2.75–2.99 (m, 2H, $H_{2'}$-$H_{6'}$, pip.) 3.48 (d, 2H, CH_2); 3.65 (s, 2H, N–CH_2–phenyl); 7.24–7.82 (m, 9H, arom.); 8.21 (s, 1H, N=C*H*–Ar). MS: *m*/*z* 327 [MH^+], 328 [MH^+ + 2].

***N*-(4-Chlorobenzylidene)-1-(1-(4-chlorobenzyl)-piperidin-4-yl)methanamine (5d).** IR cm^{-1} (Nujol): 1640. ^1H NMR ($CDCl_3$–TMS) ppm (δ): 1.50–1.98 (m, 5H, $H_{3,3'}$-$H_{5,5'}$-H_4, pip.); 2.20–2.31 (m, 2H, H_2-H_6, pip.); 2.85–3.10 (m, 2H, $H_{2'}$-$H_{6'}$, pip.) 3.50 (d, 2H, CH_2); 3.66 (s, 2H, N–CH_2–phenyl); 7.30–7.77 (m, 8H, arom.); 8.34 (s, 1H, N=C*H*–Ar). MS: *m*/*z* 361 [MH^+], 363 [MH^+ + 2].

***N*-(4-Methylbenzylidene)-1-(1-benzylpiperidin-4-yl)-methanamine (5e).** IR cm^{-1} (Nujol): 1638. ^1H NMR ($CDCl_3$–TMS) ppm (δ): 1.55–1.97 (m, 5H, $H_{3,3'}$-$H_{5,5'}$-H_4, pip.); 2.08–2.21 (m, 2H, H_2-H_6, pip.); 2.33 (s, 3H, CH_3); 2.70–2.93 (m, 2H, $H_{2'}$-$H_{6'}$, pip.) 3.42 (d, 2H, CH_2); 3.57 (s, 2H, N–CH_2–phenyl); 7.21–7.79 (m, 9H, arom.); 8.23 (s, 1H, N=C*H*–Ar). MS: *m*/*z* 307 [MH^+].

***N*-(4-Methylbenzylidene)-1-(1-(4-chlorobenzyl)-piperidin-4-yl)methanamine (5f).** IR cm^{-1} (Nujol): 1641. ^1H NMR ($CDCl_3$–TMS) ppm (δ): 1.56–2.03 (m, 5H, $H_{3,3'}$-$H_{5,5'}$-H_4, pip.); 2.05–2.20 (m, 2H, H_2-H_6, pip.); 2.32 (s, 3H, CH_3); 2.68–2.94 (m, 2H, $H_{2'}$-$H_{6'}$, pip.) 3.44 (d, 2H, CH_2); 3.61 (s, 2H, N–CH_2–phenyl); 7.28–7.75 (m, 8H, arom.); 8.27 (s, 1H, N=C*H*–Ar). MS: *m*/*z* 341 [MH^+], 343 [MH^+ + 2].

***N*-Benzyl-1-(1-benzylpiperidin-4-yl)methanamine (6a).** $NaBH_4$ (0.12 g, 3.42 mmol) was slowly added to a mixture of **5a** (0.50 g, 1.71 mmol) in 25 mL of MeOH. After stirring overnight, the solution was concentrated *in vacuo* and extracted with AcOEt (30 mL). The organic phase was washed with distilled water (3 × 15 mL) and then evaporated under reduced pressure, yielding **6a** as a pure pale oil; yield 0.35 g (69%). IR cm^{-1} (Nujol): 3257. ^1H NMR ($CDCl_3$–TMS) ppm (δ): 1.33–1.63 (m, 5H, $H_{3,3'}$-$H_{5,5'}$-H_4, pip.); 1.88–2.05 (m, 3H, H_2-H_6, pip. + N*H* disappearing on deuteration); 2.53 (d, 2H, CH_2); 2.80–2.93 (m, 2H, $H_{2'}$-$H_{6'}$, pip.); 3.49 (s, 2H, N–CH_2–phenyl); 3.77 (s, 2H, NH–CH_2–phenyl); 7.23–7.50 (m, 10H, arom.). MS: *m*/*z* 295 [MH^+].

Compounds **6b–f** were obtained by reduction of the relevant intermediates by $NaBH_4$.

***N*-Benzyl-1-(1-(4-chlorobenzyl)piperidin-4-yl)-methanamine (6b).** IR cm^{-1} (Nujol): 3261. ^1H NMR ($CDCl_3$–TMS) ppm (δ): 1.38–1.71 (m, 5H, $H_{3,3'}$-$H_{5,5'}$-H_4, pip.); 1.89–2.11 (m, 3H, H_2-H_6, pip. + N*H* disappearing on deuteration); 2.51 (d, 2H, CH_2); 2.78–2.94 (m, 2H, $H_{2'}$-$H_{6'}$, pip.); 3.50 (s, 2H, N–CH_2–phenyl); 3.79 (s, 2H, NH–CH_2–phenyl); 7.23–7.62 (m, 9H, arom.). MS: *m*/*z* 329 [MH^+], 331 [MH^+ + 2].

***N*-(4-Chlorobenzyl)-1-(1-benzylpiperidin-4-yl)-methanamine (6c).** IR cm^{-1} (Nujol): 3261. ^1H NMR ($CDCl_3$–TMS) ppm (δ): 1.39–1.70 (m, 5H, $H_{3,3'}$-$H_{5,5'}$-H_4, pip.); 1.90–2.09 (m, 3H, H_2-H_6, pip. + N*H* disappearing on deuteration); 2.52 (d, 2H, CH_2); 2.81–2.93 (m, 2H, $H_{2'}$-$H_{6'}$, pip.); 3.51 (s, 2H, N–CH_2–phenyl); 3.80 (s, 2H, NH–CH_2–phenyl); 7.25–7.61 (m, 9H, arom.). MS: *m*/*z* 329 [MH^+], 331 [MH^+ + 2].

***N*-(4-Chlorobenzyl)-1-(1-(4-chlorobenzyl)piperidin-4-yl)methanamine (6d).** IR cm^{-1} (Nujol): 3261. ^1H NMR ($CDCl_3$–TMS) ppm (δ): 1.37–1.72 (m, 5H, $H_{3,3'}$-$H_{5,5'}$-H_4, pip.); 1.91–2.11 (m, 3H, H_2-H_6, pip. + N*H* disappearing on deuteration); 2.52 (d, 2H, CH_2); 2.82–2.97 (m, 2H, $H_{2'}$-$H_{6'}$, pip.); 3.52 (s, 2H, N–CH_2–phenyl); 3.77 (s, 2H, NH–CH_2–phenyl); 7.25–7.65 (m, 8H, arom.). MS: *m*/*z* 363 [MH^+], 363 [MH^+ + 2].

***N*-(4-Methylbenzil)-1-(1-benzylpiperidin-4-yl)-methanamine (6e).** IR cm^{-1} (Nujol): 3259. ^1H NMR ($CDCl_3$–TMS) ppm (δ): 1.39–1.75 (m, 5H, $H_{3,3'}$-$H_{5,5'}$-H_4, pip.); 1.88–2.10 (m, 3H, H_2-H_6, pip. + N*H* disappearing on deuteration); 2.32 (s, 3H, CH_3) 2.50 (d, 2H, CH_2); 2.80–2.99 (m, 2H, $H_{2'}$-$H_{6'}$, pip.); 3.50 (s, 2H, N–CH_2–phenyl); 3.71 (s, 2H, NH–CH_2–phenyl); 7.22–7.63 (m, 9H, arom.). MS: *m*/*z* 309 [MH^+].

***N*-(4-Methylbenzyl)-1-(1-(4-chlorobenzyl)piperidin-4-yl)methanamine (6f).** IR cm^{-1} (Nujol): 3258. ^1H NMR ($CDCl_3$–TMS) ppm (δ): 1.35–1.69 (m, 5H, $H_{3,3'}$-$H_{5,5'}$-H_4, pip.); 1.85–2.07 (m, 3H, H_2-H_6, pip. + N*H* disappearing on deuteration); 2.33 (s, 3H, CH_3) 2.47 (d, 2H, CH_2); 2.77–3.01 (m, 2H, $H_{2'}$-$H_{6'}$, pip.); 3.48 (s, 2H, N–CH_2–phenyl); 3.69 (s, 2H, NH–CH_2–phenyl); 7.26–7.68 (m, 8H, arom.). MS: *m*/*z* 343 [MH^+], 345 [MH^+ + 2].

***N*-Benzyl-*N*-((1-benzylpiperidin-4-yl)methyl)-acetamide (2a).** A solution of acetyl chloride (0.15 g, 1.90 mmol) in 5 mL of THF was added with cooling and dropwise to a solution of **6a** (0.55 g, 1.90 mmol) and triethylamine (0.23 g, 2.28 mmol) in 10 mL of THF. After 5 h, the solvent was removed at reduced pressure, and the residue was extracted with $CHCl_3$. The organic phase was washed, dried, and concentrated *in vacuo*, giving **2a** as a chromatographic pure colorless oil; yield 0.49 g (76%). IR cm^{-1} (Nujol): 1740 cm^{-1}. ^1H NMR ($CDCl_3$–TMS) ppm (δ): 1.28–1.71 (m, 5H, $H_{3,3'}$-$H_{5,5'}$-H_4, pip.); 1.85–2.07 (m, 2H, H_2-H_6, pip.); 2.29 (s, 3H, –CO–CH_3); 2.77–3.01 (m, 2H, $H_{2'}$-$H_{6'}$, pip.); 3.27 (d, 2H, CH_2); 3.49 (s, 2H, N–CH_2–phenyl); 4.51 (s, 2H, CO–N–CH_2–phenyl); 7.12–7.40 (m, 10H, arom.). MS: *m*/*z* 337 [MH^+].

Derivatives **2b–l** were synthesized following the same recipe, starting from the relevant intermediate **6a–f** and acetyl chloride or benzoyl chloride, respectively.

***N*-Benzyl-*N*-((1-benzylpiperidin-4-yl)methyl)-benzamide (2b).** IR cm^{-1} (Nujol): 1721 cm^{-1}. ^1H NMR ($CDCl_3$–TMS) ppm (δ): 1.29–1.75 (m, 5H, $H_{3,3'}$-$H_{5,5'}$-H_4, pip.); 1.90–2.03 (m, 2H, H_2-H_6, pip.); 2.97–3.20 (m, 2H, $H_{2'}$-$H_{6'}$, pip.); 3.46 (d, 2H, CH_2); 4.50 (s, 2H, N–CH_2–phenyl); 4.78 (s, 2H, CO–N–CH_2–phenyl); 7.11–8.02 (m, 15H, arom.). MS: *m*/*z* 399 [MH^+].

***N*-Benzyl-*N*-((1-(4-chlorobenzyl)piperidin-4-yl)-methyl)acetamide (2c).** IR cm^{-1} (Nujol): 1741 cm^{-1}. ^1H

NMR ($CDCl_3$–TMS) ppm (δ): 1.30–1.77 (m, 5H, $H_{3,3'}$-$H_{5,5'}$-H_4, pip.); 1.84–2.08 (m, 2H, H_2-H_6, pip.); 2.30 (s, 3H, –CO–CH_3); 2.75–3.00 (m, 2H, $H_{2'}$-$H_{6'}$, pip.); 3.26 (d, 2H, CH_2); 3.54 (s, 2H, N–CH_2–phenyl); 4.53 (s, 2H, CO–N–CH_2–phenyl); 7.12–7.52 (m, 9H, arom.). MS: m/z 371 [MH^+], 373 [MH^+ + 2].

***N*-Benzyl-*N*-((1-(4-chlorobenzyl)piperidin-4-yl)-methyl)benzamide (2d).** IR cm^{-1} (Nujol): 1723 cm^{-1}. ^1H NMR ($CDCl_3$–TMS) ppm (δ): 1.26–1.78 (m, 5H, $H_{3,3'}$-$H_{5,5'}$-H_4, pip.); 1.91–2.02 (m, 2H, H_2-H_6, pip.); 2.97–3.15 (m, 2H, $H_{2'}$-$H_{6'}$, pip.); 3.48 (d, 2H, CH_2); 4.46 (s, 2H, N–CH_2–phenyl); 4.81 (s, 2H, CO–N–CH_2–phenyl); 7.19–8.03 (m, 14H, arom.). MS: m/z 433 [MH^+], 435 [MH^+ + 2].

***N*-4-Chlorobenzyl-*N*-((1-benzylpiperidin-4-yl)methyl)-acetamide (2e).** IR cm^{-1} (Nujol): 17420 cm^{-1}. ^1H NMR ($CDCl_3$–TMS) ppm (δ): 1.31–1.76 (m, 5H, $H_{3,3'}$-$H_{5,5'}$-H_4, pip.); 1.83–2.06 (m, 2H, H_2-H_6, pip.); 2.31 (s, 3H, –CO–CH_3); 2.73–2.99 (m, 2H, $H_{2'}$-$H_{6'}$, pip.); 3.22 (d, 2H, CH_2); 3.50 (s, 2H, N–CH_2–phenyl); 4.59 (s, 2H, CO–N–CH_2–phenyl); 7.19–7.55 (m, 9H, arom.). MS: m/z 371 [MH^+], 373 [MH^+ + 2].

***N*-4-Chlorobenzyl-*N*-((1-benzyl)piperidin-4-yl)-methyl)benzamide (2f).** IR cm^{-1} (Nujol): 1719 cm^{-1}. ^1H NMR ($CDCl_3$–TMS) ppm (δ): 1.25–1.79 (m, 5H, $H_{3,3'}$-$H_{5,5'}$-H_4, pip.); 1.93–2.04 (m, 2H, H_2-H_6, pip.); 2.93–3.12 (m, 2H, $H_{2'}$-$H_{6'}$, pip.); 3.49 (d, 2H, CH_2); 4.43 (s, 2H, N–CH_2–phenyl); 4.77 (s, 2H, CO–N–CH_2–phenyl); 7.20–8.05 (m, 14H, arom.). MS: m/z 433 [MH^+], 435 [MH^+ + 2].

***N*-4-Chlorobenzyl-*N*-((1-(4-chlorobenzyl)piperidin-4-yl)methyl)acetamide (2g).** IR cm^{-1} (Nujol): 1738 cm^{-1}. ^1H NMR ($CDCl_3$–TMS) ppm (δ): 1.34–1.75 (m, 5H, $H_{3,3'}$-$H_{5,5'}$-H_4, pip.); 1.83–2.06 (m, 2H, H_2-H_6, pip.); 2.29 (s, 3H, –CO–CH_3); 2.75–3.03 (m, 2H, $H_{2'}$-$H_{6'}$, pip.); 3.24 (d, 2H, CH_2); 3.51 (s, 2H, N–CH_2–phenyl); 4.58 (s, 2H, CO–N–CH_2–phenyl); 7.27–7.78 (m, 8H, arom.). MS: m/z 405 [MH^+], 407 [MH^+ + 2].

***N*-4-Chlorobenzyl-*N*-((1-(4-chlorobenzyl)piperidin-4-yl)methyl)benzamide (2h).** IR cm^{-1} (Nujol): 1721 cm^{-1}. ^1H NMR ($CDCl_3$–TMS) ppm (δ): 1.29–1.80 (m, 5H, $H_{3,3'}$-$H_{5,5'}$-H_4, pip.); 1.94–2.10 (m, 2H, H_2-H_6, pip.); 2.90–3.15 (m, 2H, $H_{2'}$-$H_{6'}$, pip.); 3.52 (d, 2H, CH_2); 4.39 (s, 2H, N–CH_2–phenyl); 4.65 (s, 2H, CO–N–CH_2–phenyl); 7.23–8.02 (m, 13H, arom.). MS: m/z 467 [MH^+], 469 [MH^+ + 2].

***N*-4-Methylbenzyl-*N*-((1-benzylpiperidin-4-yl)methyl)-acetamide (2i).** IR cm^{-1} (Nujol): 1736 cm^{-1}. ^1H NMR ($CDCl_3$–TMS) ppm (δ): 1.31–1.77 (m, 5H, $H_{3,3'}$-$H_{5,5'}$-H_4, pip.); 1.82–2.01 (m, 2H, H_2-H_6, pip.); 2.32 (s, 3H, –CO–CH_3); 2.33 (s, 3H, CH_3); 2.75–3.02 (m, 2H, $H_{2'}$-$H_{6'}$, pip.); 3.21 (d, 2H, CH_2); 3.46 (s, 2H, N–CH_2–phenyl); 4.46 (s, 2H, CO–N–CH_2–phenyl); 7.12–7.51 (m, 9H, arom.). MS: m/z 351 [MH^+].

***N*-4-Methylbenzyl-*N*-((1-benzylpiperidin-4-yl)methyl)-benzamide (2j).** IR cm^{-1} (Nujol): 1718 cm^{-1}. ^1H NMR ($CDCl_3$–TMS) ppm (δ): 1.26–1.80 (m, 5H, $H_{3,3'}$-$H_{5,5'}$-H_4, pip.); 1.92–2.05 (m, 2H, H_2-H_6, pip.); 2.33 (s, 3H, CH_3); 2.91–3.12 (m, 2H, $H_{2'}$-$H_{6'}$, pip.); 3.42 (d, 2H, CH_2); 4.49 (s, 2H, N–CH_2–phenyl); 4.72 (s, 2H, CO–N–CH_2–phenyl); 7.18–8.01 (m, 14H, arom.). MS: m/z 413 [MH^+].

***N*-4-Methylbenzyl-*N*-((1-(4-chlorobenzyl)piperidin-4-yl)methyl)acetamide (2k).** IR cm^{-1} (Nujol): 1741 cm^{-1}. ^1H NMR ($CDCl_3$–TMS) ppm (δ): 1.36–1.81 (m, 5H, $H_{3,3'}$-$H_{5,5'}$-H_4, pip.); 1.86–2.03 (m, 2H, H_2-H_6, pip.); 2.33 (s, 6H, CH_3); 2.71–3.04 (m, 2H, $H_{2'}$-$H_{6'}$, pip.); 3.22 (d, 2H, CH_2); 3.49 (s, 2H, N–CH_2–phenyl); 4.51 (s, 2H, CO–N–CH_2–phenyl); 7.25–7.76 (m, 8H, arom.). MS: m/z 385 [MH^+], 387 [MH^+ + 2].

***N*-4-Methylbenzyl-*N*-((1-(4-chlorobenzyl)piperidin-4-yl)methyl)benzamide (2l).** IR cm^{-1} (Nujol): 1722 cm^{-1}. ^1H NMR ($CDCl_3$–TMS) ppm (δ): 1.31–1.78 (m, 5H, $H_{3,3'}$-$H_{5,5'}$-H_4, pip.); 1.91–2.15 (m, 2H, H_2-H_6, pip.); 2.34 (s, 3H, CH_3); 2.93–3.18 (m, 2H, $H_{2'}$-$H_{6'}$, pip.); 3.48 (d, 2H, CH_2); 4.36 (s, 2H, N–CH_2–phenyl); 4.71 (s, 2H, CO–N–CH_2–phenyl); 7.26–8.06 (m, 13H, arom.). MS: m/z 447 [MH^+], 449 [MH^+ + 2].

Pharmacology. Radioligand Binding Assays. Binding assays were carried out on rat liver membranes according to the methods originally proposed by Hellewell[34] and subsequently slightly modified, as described previously.[33] Concisely, 250 μg of rat liver homogenate was incubated with 1 nM [^{3}H]-(+)-pentazocine (PerkinElmer, specific activity 34.9 Ci/mmol) for 120 min at 37 °C in 50 mM Tris-HCl, at pH 8.0, 0.5 mL final volume. Nonspecific binding was defined in the presence of 10 μM haloperidol. The reaction was stopped by vacuum filtration through GF/B glass-fiber filters presoaked with 0.5% polyethylenimine, followed by rapid washing with 2 mL of ice-cold buffer. The filters were located in 3 mL of scintillation cocktail, and the radioactivity was detected by liquid scintillation counting. At least 11 different ligand concentrations were used to perform the competition studies. Three increasing concentrations of unlabeled (+)-pentazocine were permanently included as an internal control. The compounds, previously prepared as 10 mM stock solutions in 100% DMSO, were diluted with Tris-HCl buffer on the day of the experiment. The final DMSO concentration in the incubation tubes was maintained at 0.1%. The competition data for two to four separate determinations performed in duplicate were averaged by fitting to a four parameter curve by means of the SigmaPlot software. Calculated IC_{50} values are extrapolated, and the corresponding $K_i(\sigma_1)$ values, obtained by the Cheng–Prusoff equation,[33] were reported as mean values ± SEM.

■ ASSOCIATED CONTENT

Supporting Information

Additional figures (SI1, SI2, and SI3) and elemental analysis of all compounds. This material is available free of charge via the Internet at http://pubs.acs.org.

■ AUTHOR INFORMATION

Corresponding Author

*Molecular Simulation Engineering (MOSE) Laboratory, Department of Industrial Engineering and Information Technology, University of Trieste, Via Valerio 10, 34127 Trieste, Italy. E-mail: Sabrina.Pricl@di3.units.it. Phone: +39-347-3252885. Fax: +39-040-569823.

Notes

The authors declare no competing financial interest.

■ ACKNOWLEDGMENTS

The financial support from ESTECO s.r.l. (Grant DDOS) is gratefully acknowledged. Access to CINECA supercomputing facility was granted through the sponsored Italian Super Computing Resource Allocation (ISCRA) project MONALISA.

REFERENCES

(1) Martin, W. R.; Eades, C. E.; Thompson, J. A.; Huppler, R. E.; Gilbert, P. E. The effects of morphine- and nalorphine-like drugs in the nondependent and morphine-dependent chronic spinal dog. *J. Pharmacol. Exp. Ther.* **1976**, *197*, 517−532.

(2) Bowen, W. D. Sigma receptors: recent advances and new clinical potentials. *Pharm. Acta Helv.* **2000**, *74*, 211−218.

(3) Hanner, M.; Moebius, F. F.; Flandorfer, A.; Knaus, H. G.; Striessnig, J.; Kempner, E.; Glossmann, H. Purification, molecular cloning, and expression of the mammalian sigma$_1$-binding site. *Proc. Natl. Acad. Sci. U.S.A.* **1996**, *93*, 8072−8077.

(4) Stone, J. M.; Arstad, E.; Erlandsson, K.; Waterhouse, R. N.; Ell, P. J.; Pilowsky, L. S. [^{123}I]TPCNE—a novel SPET tracer for the sigma-1 receptor: first human studies and in vivo haloperidol challenge. *Synapse* **2006**, *60*, 109−117.

(5) Cobos, E. J.; Entrena, J. M.; Nieto, F. R.; Cendan, C. M.; Pozo, E. D. Pharmacology and therapeutic potential of sigma(1) receptor ligands. *Curr. Neuropharmocol.* **2008**, *6*, 344−366.

(6) Zeng, C.; Vangveravong, S.; Jones, L. A.; Hyrc, K.; Chang, K. C.; Xu, J.; Rothfuss, J. M.; Goldberg, M. P.; Hotchkiss, R. S.; Mach, R. H. Characterization and evaluation of two novel fluorescent sigma-2 receptor ligands as proliferation probes. *Mol. Imaging* **2011**, *10*, 420−433.

(7) Kashiwagi, H.; McDunn, J. E.; Simon, P. O.; Goedegebuure, P. S.; Vangveravong, S.; Chang, K.; Hotchkiss, R. S.; Mach, R. H.; Hawkins, W. G. Sigma-2 receptor ligands potentiate conventional chemotherapies and improve survival in models of pancreatic adenocarcinoma. *J. Transl. Med.* **2009**, *7*, 24.

(8) Abate, C.; Hornick, J. R.; Spitzer, D.; Hawkins, W. G.; Niso, M.; Perrone, R.; Berardi, F. Fluorescent derivatives of σ receptor ligand 1-Cyclohexyl-4-[3-(5-methoxy-1,2,3,4-tetrahydronaphthalen-1-yl)-propyl]piperazine (PB28) as a tool for uptake and cellular localization studies in pancreatic tumor cells. *J. Med. Chem.* **2011**, *54*, 5858−5867.

(9) Monnet, F. P.; Mahé, V.; Robel, P.; Baulieu, E. E. Neurosteroids, via sigma receptors, modulate the [3H]norepinephrine release evoked by N-methyl-D-aspartate in the rat hippocampus. *Proc. Natl. Acad. Sci. U.S.A.* **1995**, *92*, 3774−3778.

(10) Waterhouse, R. N.; Collier, T. L. In vivo evaluation of [^{18}F]1-(3-fluoropropyl)-4-(4-cyanophenoxymethyl)piperidine: a selective sigma-1 receptor radioligand for PET. *Nucl. Med. Biol.* **1997**, *24*, 127−134.

(11) Fontanilla, D.; Johannessen, M.; Hajipour, A. R.; Cozzi, N. V.; Jackson, M. B.; Ruoho, A. E. The hallucinogen N,N-dimethyltryptamine (DMT) is an endogenous sigma-1 receptor regulator. *Science* **2009**, *323*, 934−937.

(12) Brimson, J.; Brown, C.; Safrany, S. T. Antagonists show GTP-sensitive high-affinity binding to the sigma-1 receptor. *Br. J. Pharmacol.* **2011**, *164*, 772−780.

(13) Maurice, T.; Su, T. P. The pharmacology of sigma-1 receptors. *Pharmacol. Ther.* **2009**, *124*, 195−206.

(14) Prasad, P. D.; Li, H. W.; Fei, Y. J.; Ganapathy, M. E.; Fujita, T.; Plumley, L. H.; Yang-Feng, T. L.; Leibach, F. H.; Ganapathy, V. Exon−intron Structure, Analysis of promoter region, and chromosomal localization of the human type 1 sigma receptor gene. *J. Neurochem.* **1998**, *70*, 443−451.

(15) Kekuda, R.; Prasad, P. D.; Fei, Y. J.; Leibach, F. H.; Ganapathy, V. Cloning and functional expression of the human type 1 sigma teceptor (hSigmaR1). *Biochem. Biophys. Res. Commun.* **1996**, *229*, 553−558.

(16) Aydar, E.; Palmer, C. P.; Klyachko, V. A.; Jackson, M. B. The sigma receptor as a ligand-regulated auxiliary potassium channel subunit. *Neuron* **2002**, *34*, 399−410.

(17) Laurini, E.; Col, V. D.; Mamolo, M. G.; Zampieri, D.; Posocco, P.; Fermeglia, M.; Vio, L.; Pricl, S. Homology model and docking-based virtual screening for ligands of the σ_1 receptor. *ACS Med. Chem. Lett.* **2011**, *2*, 834−839.

(18) Seth, P.; Ganapathy, M. E.; Conway, S. J.; Bridges, C. D.; Smith, S. B.; Casellas, P.; Ganapathy, V. Expression pattern of the type 1 sigma receptor in the brain and identity of critical anionic amino acid residues in the ligand-binding domain of the receptor. *Biochim. Biophys. Acta* **2001**, *1540*, 59−67.

(19) Zampieri, D.; Mamolo, M. G.; Laurini, E.; Florio, C.; Zanette, C.; Fermeglia, M.; Posocco, P.; Paneni, M. S.; Pricl, S.; Vio, L. Synthesis, biological evaluation, and three-dimensional in silico pharmacophore model for σ1 receptor ligands based on a series of substituted benzo[d]oxazol-2(3H)-one derivatives. *J. Med. Chem.* **2009**, *52*, 5380−5393.

(20) Laurini, E.; Zampieri, D.; Mamolo, M. G.; Vio, L.; Zanette, C.; Florio, C.; Posocco, P.; Fermeglia, M.; Pricl, S. A 3D-pharmacophore model for sigma2 receptors based on a series of substituted benzo[d]oxazol-2(3H)-one derivatives. *Bioorg. Med. Chem. Lett.* **2010**, *20*, 2954−2957.

(21) Srinivasan, J.; Cheatham, T. E., III; Cieplak, P.; Kollman, P. A.; Case, D. A. Continuum solvent studies of the stability of DNA, RNA and phosphoramidate-DNA helices. *J. Am. Chem. Soc.* **1998**, *120*, 9401−9409.

(22) (a) Pal, A.; Fontanilla, A. R.; Ramachandran, S.; Chu, U. B.; Mavlyutov, T.; Ruoho, A. E. Identification of regions of the sigma-1 receptor ligand binding site using a novel photoprobe. *Mol. Pharmacol.* **2007**, *72*, 921−933. (b) Pal, A.; Chu, U. B.; Ramachandran, S.; Grawoig, D.; Guo, L. W.; Hajipour, A. R.; Ruoho, A. E. Juxtaposition of the steroid binding domain-like I and II regions constitutes a ligand binding site in the σ-1 receptor. *J. Biol. Chem.* **2008**, *283*, 19646−19656.

(23) For a list of recent, successful applications of the MM/PBSA methodology in related topics from our group, see, for instance: (a) Carta, A.; Briguglio, I.; Piras, S.; Boatto, G.; La Colla, P.; Loddo, R.; Tolomeo, M.; Grimaudo, S.; Di Cristina, A.; Pipitone, R. M.; Laurini, E.; Paneni, M. S.; Posocco, P.; Fermeglia, M.; Pricl, S. 3-Aryl-2-[1H-benzotriazol-1-yl]acrylonitriles: a novel class of potent tubulin inhibitors. *Eur. J. Med. Chem.* **2011**, *46*, 4151−4167. (b) Liu, X.; Chen, H.; Laurini, E.; Wang, Y.; Dal Col, V.; Posocco, P.; Ziarelli, F.; Fermeglia, M.; Zhang, C. C.; Pricl, S.; Peng, L. 2-difluoromethylene-4-methylenepentanoic acid, a paradoxical probe able to mimic the signaling role of 2-oxoglutaric acid in cyanobacteria. *Org. Lett.* **2011**, *13*, 2924−2927. (c) Giliberti, G.; Ibba, C.; Marongiu, E.; Loddo, R.; Tonelli, M.; Boido, V.; Laurini, E.; Posocco, P.; Fermeglia, M.; Pricl, S. Synergistic experimental/computational studies on arylazoenamine derivatives that target the bovine viral diarrhea virus RNA-dependent RNA polymerase. *Bioorg. Med. Chem.* **2010**, *18*, 6055−6068. (d) Tonelli, M.; Boido, V.; La Colla, P.; Loddo, R.; Posocco, P.; Paneni, M. S.; Fermeglia, M.; Pricl, S. Pharmacophore modeling, resistant mutant isolation, docking, and MM-PBSA analysis: Combined experimental/computer-assisted approaches to identify new inhibitors of the bovine viral diarrhea virus (BVDV). *Bioorg. Med. Chem.* **2010**, *18*, 2304−2316. (e) Carta, A.; Pricl, S.; Piras, S.; Fermeglia, M.; La Colla, P.; Loddo, R. Activity and molecular modeling of a new small molecule active against NNRTI-resistant HIV-1 mutants. *Eur. J. Med. Chem.* **2009**, *44*, 5117−5122. (f) Tonelli, M.; Vazzana, I.; Tasso, B.; Boido, V.; Sparatore, F.; Fermeglia, M.; Paneni, M. S.; Posocco, P.; Pricl, S.; La Colla, P.; Ibba, C.; Secci, B.; Collu, G.; Loddo, R. Antiviral and cytotoxic activities of aminoarylazo compounds and aryltriazene derivatives. *Bioorg. Med. Chem.* **2009**, *17*, 4425−4440 and references therein.

(24) (a) Liu, X.; Liu, C.; Laurini, E.; Posocco, P.; Pricl, S.; Qu, F.; Rocchi, P.; Peng, L. Efficient delivery of sticky siRNA and potent gene silencing in a prostate cancer model using a generation 5 triethanolamine-core PAMAM dendrimer. *Mol. Pharmaceutics* **2012**, *9*, 470−481. (b) Karatasos, K.; Posocco, P.; Laurini, E.; Pricl, S. Poly(amidoamine)-based dendrimer/siRNA complexation studied by computer simulations: effects of pH and generation on dendrimer structure and siRNA binding. *Macromol. Biosci.* **2012**, *12*, 225−240. (c) Liu, X.; Wu, J.; Yammine, M.; Zhou, J.; Posocco, P.; Viel, S.; Liu, C.; Ziarelli, F.; Fermeglia, M.; Pricl, S.; Victorero, G.; Nguyen, C.; Erbacher, P.; Behr, J. P.; Peng, L. Structurally flexible triethanolamine core PAMAM dendrimers are effective nanovectors for DNA transfection in vitro and in vivo to the mouse thymus. *Bioconjugate Chem.* **2011**, *22*, 2461−7243. (d) Barnard, A.; Posocco, P.; Pricl, S.;

Calderon, M.; Haag, R.; Hwang, M. E.; Shum, V. W.; Pack, D. W.; Smith, D. K. Degradable self-assembling dendrons for gene delivery: experimental and theoretical insights into the barriers to cellular uptake. *J. Am. Chem. Soc.* **2011**, *133*, 20288−20300. (e) Pierotti, M. A.; Tamborini, E.; Negri, T.; Pricl, S.; Pilotti, S. Targeted therapy in GIST: in silico modeling for prediction of resistance. *Nat. Rev. Clin. Oncol.* **2011**, *8*, 161−170. (f) Pavan, G. M.; Posocco, P.; Tagliabue, A.; Maly, M.; Malek, A.; Danani, A.; Ragg, E.; Catapano, C. V.; Pricl, S. PAMAM dendrimers for siRNA delivery: computational and experimental insights. *Chem.—Eur. J.* **2010**, *16*, 7781−7795. (g) Dileo, P.; Pricl, S.; Tamborini, E.; Negri, T.; Stacchiotti, S.; Gronchi, A.; Posocco, P.; Laurini, E.; Coco, P.; Fumagalli, E.; Casali, P. G.; Pilotti, S. Imatinib response in two GIST patients carrying two hitherto functionally uncharacterized PDGFRA mutations: an imaging, biochemical and molecular modeling study. *Int. J. Cancer* **2011**, *128*, 983−990. (h) Jones, S. P.; Pavan, G. M.; Danani, A.; Pricl, S.; Smith, D. K. Quantifying the effect of surface ligands on dendron-DNA interactions: insights into multivalency through a combined experimental and theoretical approach. *Chem.—Eur. J.* **2010**, *16*, 4519−4532. (i) Pierotti, M. A.; Negri, T.; Tamborini, E.; Perrone, F.; Pricl, S.; Pilotti, S. Targeted therapies: the rare cancer paradigm. *Mol. Oncol.* **2010**, *4*, 19−37. (j) Conca, E.; Negri, T.; Gronchi, A.; Fumagalli, E.; Tamborini, E.; Pavan, G. M.; Fermeglia, M.; Pierotti, M. A.; Pricl, S.; Pilotti, S. Activate and resist: L576P-KIT in GIST. *Mol. Cancer Ther.* **2009**, *8*, 2491−2495. (k) Woodman, S. E.; Trent, J. C.; Stemke-Hale, K.; Lazar, A. J.; Pricl, S.; Pavan, G. M.; Fermeglia, M.; Gopal, Y. N.; Yang, D.; Podoloff, D. A.; Ivan, D.; Kim, K. B.; Papadopoulos, N.; Hwu, P.; Mills, G. B.; Davies, M. A. Activity of dasatinib against L576P KIT mutant melanoma: molecular, cellular, and clinical correlates. *Mol. Cancer Ther.* **2009**, *8*, 2079−2085. (l) Pavan, G. M.; Danani, A.; Pricl, S.; Smith, D. K. Modeling the multivalent recognition between dendritic molecules and DNA: understanding how ligand "sacrifice" and screening can enhance binding. *J. Am. Chem. Soc.* **2009**, *131*, 9686−9694 and references therein.

(25) Selzer, T.; Albeck, S.; Schreiber, G. Rational design of faster associating and tighter binding protein complexes. *Nat. Struct. Biol.* **2000**, *7*, 537−541.

(26) Sulea, T.; Purisima, E. O. Optimizing ligand charges for maximum binding affinity. A solvated interaction energy approach. *J. Phys. Chem. B* **2001**, *105*, 889−899.

(27) Kangas, E.; Tidor, B. Optimizing electrostatic affinity in ligand-receptor binding: Theory, computation, and ligand properties. *J. Chem. Phys.* **1998**, *109*, 7522−7545.

(28) Lee, L. P.; Tidor, B. Optimization of binding electrostatics: charge complementarity in the barnase-barstar protein complex. *Protein Sci.* **2001**, *10*, 362−377.

(29) Gohlke, H.; Kiel, C.; Case, D. A. Insights into protein-protein binding by binding free energy calculation and free energy decomposition for the Ras-Raf and Ras-RalGDS complexes. *J. Mol. Biol.* **2003**, *330*, 891−913.

(30) Massova, I.; Kollman, P. A. Computational alanine scanning to probe protein-protein interactions: A novel approach to evaluate binding free energies. *J. Am. Chem. Soc.* **1999**, *121*, 8133−8143.

(31) Huo, S.; Massova, I.; Kollman, P. A. Computational alanine scanning of the 1:1 human growth hormone-receptor complex. *J. Comput. Chem.* **2002**, *23*, 15−27.

(32) Palmer, C. P.; Mahen, R.; Schnell, E.; Djamgoz, M. B. A.; Aydar, E. Sigma-1 receptors bind cholesterol and remodel lipid rafts in breast cancer cell lines. *Cancer Res.* **2007**, *67*, 11166−11175.

(33) Zampieri, D.; Mamolo, M. G.; Laurini, E.; Zanette, C.; Florio, C.; Collina, S.; Urbano, M.; Azzolina, O.; Vio, L. Substituted benzo[d]oxazol-2(3H)-one derivatives with preference for the sigma1 binding site. *Eur. J. Med. Chem.* **2009**, *44*, 124−30.

(34) Hellewell, S. B.; Bruce, A.; Feinstein, G.; Orringer, J.; Williams, W.; Bowen, W. D. Rat liver and kidney contain high densities of sigma 1 and sigma 2 receptors: characterization by ligand binding and photoaffinity labeling. *Eur. J. Pharmacol.* **1994**, *268*, 9−18.

(35) Martin, W. R.; Eades, C. E.; Thompson, J. A.; Huppler, R. E. The effects of morphine- and nalorphine-like drugs in the non-dependent and morphine-dependent chronic spinal dog. *J. Pharmacol. Exp. Ther.* **1976**, *197*, 517−532.

(36) Morris, G. M.; Huey, R.; Lindstrom, W.; Sanner, M. F.; Belew, R. K.; Goodsell, D. S.; Olson, A. J. AutoDock4 and AutoDockTools4: Automated docking with selective receptor flexibility. *J. Comput. Chem.* **2009**, *30*, 2785−2791.

(37) Mehler, E. L.; Solmajer, T. Electrostatic effects in proteins: comparison of dielectric and charge models. *Protein Eng.* **1991**, *4*, 903−910.

(38) (a) Onufriev, A.; Bashford, D.; Case, D. A. Modification of the generalized born model suitable **for** macromolecules. *J. Phys. Chem. B* **2000**, *104*, 3712−3720. (b) Feig, M.; Onufriev, A.; Lee, M. S.; Im, W.; Case, D. A.; Brooks, C. L. Performance comparison of generalized born and Poisson methods in the calculation of electrostatic solvation energies for protein structures. *J. Comput. Chem.* **2004**, *25*, 265−284.

(39) Case, D. A.; Darden, T. A.; Cheatham, T. E., III.; Simmerling, C. L.; Wang, J.; Duke, R. E.; Luo, R.; Walker, R. C.; Zhang, W.; Merz, K. M.; Roberts, B.; Wang, B.; Hayik, S.; Roitberg, A.; Seabra, G.; Kolossváry, I.; Wong, K. F.; Paesani, F.; Vanicek, J.; Wu, X.; Brozell, S. R.; Steinbrecher, T.; Gohlke, H.; Cai, Q.; Ye, X.; Wang, J.; Hsieh, M.-J.; Cui, G.; Roe, D. R.; Mathews, D. H.; Seetin, M. G.; Sagui, C.; Babin, V.; Luchko, T.; Gusarov, S.; Kovalenko, A.; Kollman, P. A. *AMBER 11*; University of California: San Francisco, CA, USA, 2010.

(40) (a) Felluga, F.; Pitacco, G.; Valentin, E.; Coslanich, A.; Fermeglia, M.; Ferrone, M.; Pricl, S. Studying enzyme enantioselectivity using combined ab initio and free energy calculations: α-chymotrypsin and methyl cis- and trans-5-oxo-2-pentylpirrolidine-3-carboxylates. *Tetrahedron: Asymmetry* **2003**, *14*, 3385−3399. (b) Frecer, V.; Kabeláč, M.; De Nardi, P.; Pricl, S.; Miertuš, S. Structure-based design of inhibitors of NS3 serine protease of hepatitis C virus. *J. Mol. Graphics Modell.* **2004**, *22*, 209−220.

(41) Jakalian, A.; Bush, B. L.; Jack, D. B.; Bayly, C. I. Fast, efficient generation of high-quality atomic charges. AM1-BCC model: I. Method. *J. Comput. Chem.* **2000**, *21*, 132−146.

(42) Duan, Y.; Wu, C.; Chowdhury, S.; Lee, M. C.; Xiong, G.; Zhang, W.; Yang, R.; Cieplak, P.; Luo, R.; Lee, T.; Caldwell, J.; Wang, J.; Kollman, P. A. Point-charge force field for molecular mechanics simulations of proteins based on condensed-phase quantum mechanical calculations. *J. Comput. Chem.* **2003**, *24*, 1999−2012.

(43) Wang, J.; Wolf, R. M.; Caldwell, J. W.; Kollman, P. A.; Case, D. A. Development and testing of a general amber force field. *J. Comput. Chem.* **2004**, *25*, 1157−1174.

(44) Jorgensen, W. L.; Chandrasekhar, J.; Madura, J. D.; Impey, R. W.; Klein, M. L. Comparison of simple potential functions for simulating liquid water. *J. Chem. Phys.* **1983**, *79*, 926−935.

(45) Ryckaert, J.-P.; Ciccotti, G.; Berendsen, H. J. C. Numerical integration of the cartesian equations of motion of a system with constraints: molecular dynamics of n-alkanes. *J. Comput. Phys.* **1977**, *23*, 327−341.

(46) Toukmaji, A.; Sagui, C.; Board, J.; Darden, T. Efficient particle-mesh Ewald based approach to fixed and induced dipolar interactions. *J. Chem. Phys.* **2000**, *113*, 10913−10927.

(47) Gilson, M. K.; Sharp, K. A.; Honig, B. H. Calculating the electrostatic potential of molecules in solution: Method and error assessment. *J. Comput. Chem.* **1988**, *9*, 327−335.

(48) Sitkoff, D.; Sharp, K. A.; Honig, B. Accurate calculation of hydration free energies using macroscopic solvent models. *J. Phys. Chem.* **1994**, *98*, 1978−1988.

(49) Sanner, M. F.; Olson, A. J.; Spehner, J. C. Reduced surface: an efficient way to compute molecular surfaces. *Biopolymers* **1996**, *38*, 305−320.

(50) Wilson, E. B.; Decius, J. C.; Cross, P. C. *Molecular Vibrations*; McGraw-Hill: New York, NY, 1995.

(51) Tsui, V.; Case, D. A. Theory and applications of the Generalized Born solvation model in macromolecular simulations. *Biopolymers* **2000**, *56*, 275−291.

(52) Zoete, V.; Michielin, O. Comparison between computational alanine scanning and per-residue binding free energy decomposition for protein-protein association using MM-GBSA: Application to the TCR-p-MHC complex. *Proteins* **2007**, *67*, 1026−1047.
(53) Guo, J.; Wang, X.; Sun, H.; Liu, H.; Yao, X. The molecular basis of IGF-II/IGF2R recognition: a combined molecular dynamics simulation, free-energy calculation and computational alanine scanning study. *J. Mol. Model.* **2011**, 1−10.
(54) Moreira, I. S.; Fernandes, P. A.; Ramos, M. J. Computational alanine scanning mutagenesis—An improved methodological approach. *J. Comput. Chem.* **2006**, *28*, 644−654.
(55) http://www.esteco.com/home/mode_frontier/mode_frontier.html.